

# POLITECNICO DI TORINO

Department of Mechanical and Aerospace Engineering  
Master in Automotive Engineering



**Politecnico  
di Torino**



**SQUADRA | CORSE**  
POLITO

Master 's Degree Thesis

**Upright's design using additive  
manufacturing for a formula student car**

**Tutor**

**Candidate**

**Prof. Andrea TONOLI**

**Francesco MONTE**

**Academic Year 2024/2025**

# Acknowledgements

## ACKNOWLEDGMENTS

*A Marzia e Peppe che mi hanno guidato e supportato.*

*A Luigi che mi ha aiutato e ha vissuto con me.*

*A Martina e Luigi che hanno vegliato su di me.*

*Agli amici che mi sono stati vicini e che hanno reso le mie giornate più felici.*

*Ai ragazzi di MNS e di SC con cui abbiamo condiviso più di una passione.*

*A tutti coloro che ho incontrato in questi anni universitari.*

*E a Martina che è stata un punto di riferimento.*

# Table of Contents

<b>List of Tables</b>	IV
<b>List of Figures</b>	VI
<b>Acronyms</b>	IX
<b>1 Introduction</b>	2
1.1 Formula Student . . . . .	2
1.2 Squadra Corse PoliTo . . . . .	4
1.3 Unsprung Masses Division . . . . .	7
<b>2 SC24 Upright system</b>	10
2.1 2021 season . . . . .	10
2.2 2022 season . . . . .	12
2.2.1 Production technology and material . . . . .	12
2.2.2 Component characteristics . . . . .	15
2.3 Why additive manufacturing? . . . . .	17
<b>3 Design targets</b>	19
3.1 Stiffness . . . . .	20
3.1.1 Stiffness targets . . . . .	22
3.2 Reliability . . . . .	25
3.2.1 Reliability target . . . . .	25
3.3 Weight . . . . .	26
3.3.1 Weight targets . . . . .	27
<b>4 Component design</b>	28
4.1 Load cases . . . . .	28
4.1.1 Design load cases . . . . .	29
4.1.2 Verification load cases . . . . .	29
4.2 Loads model . . . . .	30

4.3	Fatigue study . . . . .	35
4.3.1	Fatigue load case . . . . .	35
<b>5</b>	<b>FEM models</b>	<b>37</b>
5.1	FEM model for structural analysis . . . . .	37
5.1.1	Reliability FEM model . . . . .	39
5.1.2	Stiffness FEM model . . . . .	41
5.2	Topology optimization . . . . .	43
5.2.1	Topology optimization model . . . . .	45
5.3	Fatigue analysis . . . . .	46
<b>6</b>	<b>Design for Additive Manufacturing</b>	<b>51</b>
6.1	Processes and Materials for Additive Manufacturing . . . . .	52
6.1.1	Best practice for Additive Manufacturing . . . . .	53
6.1.2	Metallic materials for Additive Manufacturing . . . . .	57
6.1.3	Post processing of an Additive Manufacturing component . .	59
<b>7</b>	<b>Results</b>	<b>61</b>
7.1	Topology optimization results . . . . .	61
7.2	Reliability model results . . . . .	64
7.2.1	Verification analysis results . . . . .	70
7.3	Stiffness model results . . . . .	72
7.4	Fatigue analysis results . . . . .	74
<b>8</b>	<b>Final considerations and future works</b>	<b>76</b>
	<b>Bibliography</b>	<b>78</b>

# List of Tables

2.1	Ergal's mechanical characteristics[2]. . . . .	13
2.2	AlSi10Mg's mechanical characteristics. . . . .	14
2.3	Additional AlSi10Mg's characteristics. . . . .	14
2.4	Specimen's mechanical characteristics. . . . .	15
3.1	Maximum variation of the wheel angles allowed by design choice. . .	23
3.2	Allowed variation of wheel angle with respect to $F_x, F_y, F_z$ . . . . .	23
3.3	Variations of characteristics angle concerning the forces due to the upright in the SC24. . . . .	24
3.4	Variations of characteristics angle concerning the forces of the complete wheel assembly in the SC24. . . . .	24
3.5	Upright contribution of the allowed variation of wheel angle concerning $F_x, F_y, F_z$ . . . . .	25
3.6	Reliability targets summary . . . . .	26
3.7	SC22 and SC21 upright front weight . . . . .	27
4.1	Input data for the design load cases for the front upright . . . . .	29
4.2	Bump load case input force to be added to the design load case . .	30
4.3	Summary of all the computed loads for the front upright . . . . .	34
5.1	Coordinates of the three points used to compute the angle variations	42
6.1	Scalmalloy mechanical characteristics. . . . .	58
6.2	Ti64 Grade 5 mechanical characteristics. . . . .	58
7.1	Comparison between the optimized upright'weight concerning the SC 24 one . . . . .	63
7.2	Results sum up of the peak stresses for the three different load case	67
7.3	Safety factor for the three load cases . . . . .	67
7.4	Safety factor for the pure braking load case after the variation . . .	69
7.5	Safety factor for the three load cases verification model . . . . .	70
7.6	Coordinates of the three points after the deformation Fx load case .	72

7.7	Coordinates of the three points after the deformation Fy load case .	72
7.8	Coordinates of the three points after the deformation Fz load case .	74
7.9	Camber variation concerning the forces in the three directions x, y, and z respect to the targets . . . . .	74
7.10	Toe variation concerning the forces in the three directions x, y, and z respect to the targets . . . . .	74

# List of Figures

1.1	SC24 during the Endurance event at FSG 2024 . . . . .	3
1.2	Team photo during SC24 presentation event . . . . .	4
1.3	SC24 during skidpad event at FSG 2024 . . . . .	5
1.4	Team photo FSA . . . . .	6
1.5	Team photo FSG . . . . .	6
1.6	Unsprung masses CAD view . . . . .	8
1.7	Unsprung masses division members . . . . .	9
2.1	The SC21 upright after the 3D printing. . . . .	10
2.2	SC21 upright fail. . . . .	11
2.3	T6 temperature-time diagram. . . . .	13
2.4	SC24 wheel assembly: we can see the upright, the suspension arms, the brake system made by caliper and disk, the e-motor, and the hub.	16
2.5	Upright's inner part with only the ring gear, the hub, and the bearing with its oil seal (cannot be seen from this angle). In the front are the holes and the face that connect the motor plate. . . . .	17
2.6	A flip-chip mounted on the upright, we can see the loop shape of the component. . . . .	18
3.1	Flowchart design steps. . . . .	19
4.1	Upright reference frame and car reference frame . . . . .	31
4.2	Mx transport moment computation example . . . . .	32
4.3	Brake loads computation example . . . . .	33
4.4	Reaction on the upright of a simulated autocross lap . . . . .	36
5.1	RBE2 and single point constraint applied in the FEM model . . . . .	39
5.2	RBE3 and forces applied to the bearing center in the FEM model . . . . .	40
5.3	RBE3 and forces applied in the lateral direction . . . . .	40
5.4	Caliper forces and RBE3 applied in the FEM model . . . . .	41
5.5	RBE3 connection between the upright and the point where the displacements are measured . . . . .	43

5.6	Stiffness model in Hypermesh . . . . .	43
5.7	Starting model for topology optimization, in grey the non-design space and in brick red design space . . . . .	46
5.8	Optimization model in Inspire. Constraints, loads, and 1-D elements are applied to the gray part, the non-design space. The blue plane is the overhang constraint. . . . .	47
5.9	Fatigue analysis FEM model. All the loads and RBE3 are applied .	48
5.10	Haigh Diagram and Mean Stress Correction Methods . . . . .	48
5.11	Load cycle before and after Rainflow arrangement . . . . .	49
5.12	Gerber Safety Factor . . . . .	50
6.1	Schematization of a Laser Powder Bed Fusion process . . . . .	53
7.1	Final upright model . . . . .	61
7.2	Final upright model lateral view . . . . .	62
7.3	Von Mises stress [MPa] for the pure braking load case . . . . .	64
7.4	Signed Von Mises stress [MPa] pure braking load case . . . . .	65
7.5	Deformation results pure braking load case . . . . .	65
7.6	Von Mises stress [MPa] for the pure lateral load case . . . . .	66
7.7	Von Mises stress [MPa] for the braking in turn load case . . . . .	66
7.8	Deformation results pure lateral load case . . . . .	67
7.9	Stress components in the pure braking load case . . . . .	68
7.10	Geometry variation to reduce the stresses in the pure braking load case . . . . .	69
7.11	Von Mises stresses in the pure braking load case after the variation	69
7.12	Von Mises stress in the verification load case . . . . .	71
7.13	Displacements results of the stiffness model . . . . .	73
7.14	Fatigue analysis results . . . . .	75



# Acronyms

**SAE**

Society of Automotive Engineering

**FSA**

Formula Student Austria

**FSG**

Formula Student Germany

**FSATA**

Formula SAE Italy

**FE**

Finite Element

**FEM**

Finite Element Method

**FEA**

Finite Element Analysis

**SF**

Safety factor

**PA**

Pure acceleration

**PB**

Pure braking

**PL**

Pure lateral

**AIT**

Acceleration in turn

**BIT**

Braking in turn

**AM**

Additive Manufacturing

**DfAM**

Design for Additive Manufacturing

**CAD**

Computer Aided Design

**PBF**

Powder bed fusion

**HM**

Hybrid Manufacturing

**S-N**

Stress range - Number of cycles



## Abstract

This thesis focuses on the design of a Formula Student car upright optimized for additive manufacturing. The design process begins by analyzing the previous iteration, which was manufactured using conventional production methods, highlighting its advantages and limitations. This initial evaluation serves as the foundation for determining whether additive manufacturing presents a viable alternative, considering the project's specific targets and constraints.

Once the manufacturing approach is selected, the design objectives are defined, with a primary focus on achieving an optimal balance of stiffness, reliability, and weight. To accurately determine the forces acting on the component, various load cases are introduced, representing critical vehicle dynamics such as cornering, braking, acceleration, and combined scenarios. For each load case, input loads and contact patch coordinates are identified, enabling the calculation of forces through a dedicated physical model. Additionally, geometric constraints are established to accommodate the surrounding components within the wheel assembly.

With the design targets and loading conditions set, a custom finite element model (FEM) is developed to evaluate the component's performance. Prior to detailed FEM analysis, a topology optimization study is conducted to identify stress-concentrated regions and eliminate unnecessary material, thereby minimizing weight while maintaining structural integrity. Special consideration is given to design parameters that mitigate overhangs and other limitations inherent to additive manufacturing. Throughout the process, industry best practices for additive manufacturing are applied to ensure an efficient and manufacturable design.

Following the structural assessment, FEM simulations are carried out to verify stiffness and reliability. Finally, a fatigue analysis is performed to estimate the component's lifespan and establish a maximum operating time. This study aims to demonstrate the feasibility of additive manufacturing for high-performance automotive components, offering insights into its potential benefits and limitations.



# Chapter 1

## Introduction

The design of a Formula student car is a very fascinating challenge. Students can face different engineering problems starting from the design to the production, not forgetting that also problems during the life of the vehicle can arise and should be addressed quickly and with limited resources.

Working as a team is of paramount importance too; to achieve the ultimate goal that it's not always winning but sometimes also being able to participate and improve the team are very noble aims.

In the end, the most important takeaway for a young engineer is being able to achieve a task using careful organization and implementing good engineering practices.

### 1.1 Formula Student

The Formula Student Competition, also known as Formula SAE, is a competition that gathers students from all around the world to compete against each other with their formula-type prototypes.

The rules are stated by the German organization (FSG). In each event, technical inspections are conducted to see if the car is safe, compliant with rules, and built following good engineering practices. In addition, different tests are performed to demonstrate that the car is suitable for racing.

This year, FSG's organization accepts only electric-powered vehicles, whether they are driverless or not. A category called hybrid gathers all the internal combustion engine cars that need to adopt a certain amount of electrification. Not all the race organizers banned the pure ICE cars; each race event can, indeed, adjust the rules following their will and experience.

The competition is not just a race but can be defined as an engineering competition, meaning that not only dynamic events take place but also static events.

Static events consist of:

- /// Business plan presentation**
- /// Cost and manufacturing event**
- /// Engineering design event**

In these events, you are judged by professionals, and they require deep knowledge about the vehicle. Most importantly, they asked about the reasons why your team picked a certain decision (design event) or how you managed the production of your car (cost event).

On the other hand, the dynamic events are:

- /// Acceleration**
- /// Skidpad**
- /// Autocross**
- /// Endurance and Efficiency**



**Figure 1.1:** SC24 during the Endurance event at FSG 2024

In these events, the performance of the car is evaluated in every aspect, in terms of performance, reliability, and energy usage efficiency.

## 1.2 Squadra Corse PoliTo

The team Squadra Corse Polito was founded in 2004/2005 and was one of the first student teams of the Politecnico di Torino. In 2010, the team managed to win the world championship in the category of hybrid powertrain. In 2012 was the first Italian team to exploit an electric-powered car and since then has had a fully electric vehicle.

This year, the team is composed of 80 students from all the different majors, demonstrating that building an electric car is a real challenge that connects different technical aspects.



**Figure 1.2:** Team photo during SC24 presentation event

Thus the team is divided into 10 divisions that are in charge of every aspect of the car, starting from the design to maintenance passing through production.

The car for the 2024 season was the SC24 "Andromeda", which has the following characteristics:

- ///* Mass without the driver: 217 kg
- ///* Full carbon fibre monocoque
- ///* 4WD outboard AMK electric motors independently controlled
- ///* Front mass repartition: 48 %
- ///* Wheelbase length: 1.525 m
- ///* Track width: 1.2 m

- 🔪 Pirelli 185/40 R13 slick tires on 13" OZ Racing magnesium alloy rims
- 🔪 Aerodynamic Cl 4.9
- 🔪 Aerodynamic efficiency: 3.2
- 🔪 Maximum power 80 kW (limited by the rules)
- 🔪 0-100 km/h, 2.8 s

The SC24 respect to the previous prototype (SC22 Evo), followed the same layout configuration and main characteristics, but different parts of the car were redesigned and produced to solve previous problems and enhance performance. The SC22 Evo was a very reliable car but had some problems in terms of compliance with rules; thus, the main idea was to keep the electric and electronic parts similar and avoid spending too much money to reproduce something that already worked properly. The areas that changed the most were the chassis, the aerodynamics, and the cooling system.



**Figure 1.3:** SC24 during skidpad event at FSG 2024

During the 2024 season, the team participated in three different events: Formula Student Austria (FSA), Formula Student Germany, and Formula SAE Italy (FSATA).

Unfortunately, in the FSA event, the car didn't manage to pass the electrical inspection due to some problems that arose after an electric component failed during testing. Still, the event was very meaningful because most of the team members gained experience as that was their first race.



**Figure 1.4:** Team photo FSA

The FSG event was not too shamy; we completed all the dynamic events but the endurance. To be honest, just before the endurance event, a strong rain fell on the track, and during the first laps, the track was full of aquaplaning spots. This led to some water filtering next to the electric circuit's measuring points. Thus, during the driver change, a loss of isolation was detected, triggering a safety protocol that prevented the car from continuing. Despite the disappointment, the results were incredible because the last time Squadra Corse raced at FSG was in 2013.



**Figure 1.5:** Team photo FSG

In the FSATA event, we were able to complete all the dynamic events, scoring 13th place, which was pretty good considering the level of competition reached by the competitors. Even in this case, the car faced an endurance event with wet conditions, but thanks to the lesson learned, we were able to bring it home. The last time we completed the endurance was in the 2019 season.

In general, the team faced various obstacles, but we managed to get together and overcome them. I am proud of being a part of this team, not only for the results but mostly for the work and the dedication that put in.

### 1.3 Unsprung Masses Division

The definition of the unsprung masses or unsprung weight is [1]:

*"That part of the mass that does not change its positions concerning the ground is called the unsprung mass. Some suspension components contribute partly to sprung and partly to unsprung mass. To evaluate the two contributions, the mass of these elements must be divided into two parts, concentrated ideally in the suspension joints, in such a way as to conserve the moment of inertia and the center of gravity position."*

In Squadra Corse Polito, the unsprung masses division deals with most of the mechanical parts of the car, in particular:

- ✄ **Brake system:** two independent front and rear systems in which we design and produce the brake rotor and use Brembo brake calipers.
- ✄ **Pedalbox:** brake and throttle pedal assemblies designed and produced by us
- ✄ **Suspension and anti-roll bar:** front and rear double wishbone suspension and a torsion bar system for the anti-roll, both designed and produced on our own.
- ✄ **Steering system:** a pure mechanical steering system using a double universal joint and a pinion rack steering mechanism.
- ✄ **Upright system:** designed and produced front and rear uprights.
- ✄ **Geartrain:** two-stage planetary gear set with aluminum hub and carrier completely designed and produced by us.
- ✄ **Wheel Rims:** 13' OZ racing made in magnesium alloy.

As can be seen, some systems that are normally part of the sprung masses are also included. The main reason is due to the similar competencies that are needed to deal with these assemblies.

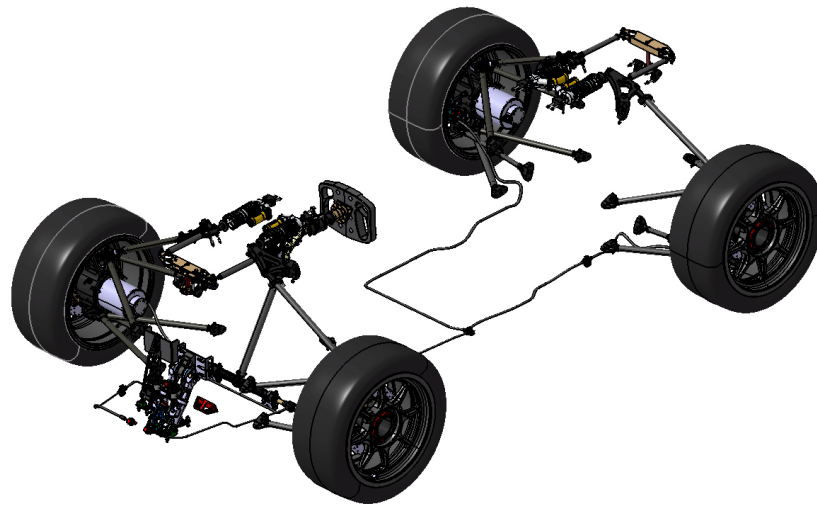


**Figure 1.6:** Unsprung masses CAD view

This year the division is composed of eleven members that came from the automotive and mechanical fields of study. The division is structured in three levels. The first one is made up of students who joined at the beginning of the season and are in charge of the design phase and redaction of technical documents. The second level comprehends the students in their second year, which provides guidance for the first-year students and takes the technical decisions regarding their field of competencies. The third level is the division leader, who manages the entire group of people, approves the decision, and reports directly to the technical director.



Figure 1.7: Unsprung masses division members

## Chapter 2

# SC24 Upright system

### 2.1 2021 season

The upright assembly used in the SC21 was designed and produced during the 2021 season. The uprights were completely redesigned using Additive manufacturing, but the results were not satisfactory due to some problems in the production processes and a failure during tests.



**Figure 2.1:** The SC21 upright after the 3D printing.

The failure occurred at the caliper boss, leading to the breakage of both the upright and the brake disk(2.2). It's still unclear whether the issue originated within the brake disk or the upright, but it's evident that design mistakes and poor engineering practices were present in both components.

Some problems present in the 2021 design were found in the following areas:

- /// Load model
- /// Material
- /// Fastener connection
- /// Post-processing



**Figure 2.2:** SC21 upright fail.

The load model did not properly take into account how the forces were transmitted from the contact patch to the component itself. Thus the FEM model underestimates the stresses in some parts, especially the ones involved in the braking.

Moreover, the connection between the brake caliper and the upright implemented a shoulder screw, as you can see in 2.2. This connection is not very often used in this type of application since the bolt is loaded in pure shear. So, the part of the material loaded was less than half. Whereas, using a simple screw and a proper tightening torque, the friction among the surfaces is capable of withstanding higher loads, and the material is better exploited.

The material was AlSi10Mg, one of the most lightweight metallic alloys used in additive manufacturing, but it came as a prize in terms of the poor strength of the material. The target of the season was reducing the weight, thus the choice of the material.

The upright, after 3D printing, is not a complete part because the production process cannot guarantee the tolerances and the surface finish needed for proper

functioning. Thus further machining is mandatory, in particular a milling process. However, due to the complex shape and characteristics, the processing was quite complex and expensive.

I will not go more in-depth about the 2021 solution, even if it's more similar to the scope of this thesis. Analyzing the SC24 solution is more important because the design process was more accurate, and eventually, the results were more satisfactory. Ultimately, the amount of data and knowledge transmitted from the 2021 season, unfortunately, was inadequate.

## 2.2 2022 season

The problems faced in the 2021 season concerned above all the production process and the strength of the material. Thus, coming back to a more traditional production process seemed the right thing to do. The design targets of the new season changed in favor of prioritizing reliability and cost reduction rather than weight and performance. Moreover, the failure of the previous year was no longer acceptable because of the lack of time and money.

All these factors contribute to the selection of the CNC milling process.

### 2.2.1 Production technology and material

By recognizing the mistakes and new goals for the 2022 season that led to the selection of a more traditional milling process, we can understand how these factors align with the characteristics of the method.

The main advantages of CNC machining are:

 **Material properties**

 **Accurate parts**

 **Quick turnaround time**

In addition, we need to consider the relative comparison with 3D printing. The main problem arose in the 2021 season regarding the needed post-processing after the 3D printing, which increases the costs and the time. Moreover, the complex shape made more difficult the component's placement in the machine, thus increasing the manufacturing cost.

The second key point change in the 2022 design was the material. The Al7075 T6 was chosen due to its ratio of strength and density. Although it's more difficult to manufacture with respect to other aluminum, such as the Al2024 and the Al6081, the difference in yield strength is quite remarkable. The Ergal (Al7075), indeed,

Properties	Values
Tensile strength	540 [MPa]
Yield strength	480 [MPa]
Young modulus	71.7 [GPa]
Elongation at break	11 [%]
Density	2.81 [ $g/cm^3$ ]
Hardness	150 [HRB]

**Table 2.1:** Ergal’s mechanical characteristics[2].

came from the aerospace sector and is known for its strength, hardness, and fatigue resistance.

It’s important to remember that the values of a material’s strength (seen in 2.1) are influenced by many factors, and where possible, these data should be provided by the supplier. Usually, they came with a certain percentage of accuracy that indicates how trustworthy that value is.

The values in 2.1 are considered after the heat treatment T6, which is the most common for structural applications. The T6 is essential and is based on solubilization, quenching, and artificial aging.

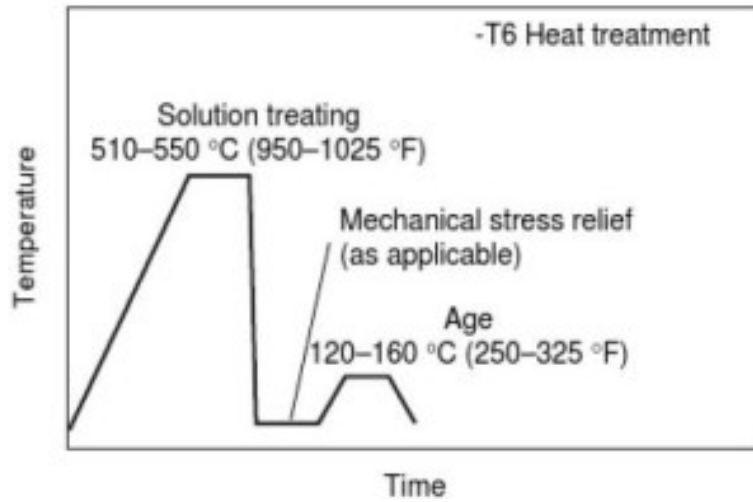


**Figure 2.3:** T6 temperature-time diagram.

As we can see in 2.3 the first part deals with the solubilization of the second phases in the alloy, which are Zn and Mg in the case of Ergal, going in solid solution.

After that, the quenching guarantees the same composition even at room

temperature. Ultimately, being the composition unstable, zones in which solute atoms are gathering will form inside the original crystal (called Guinier Preston zones).

From the Guinier Preston zones, metastable precipitates are formed, which maximize the strength.

This last phase, called aging, is the most important and can be enhanced with an increase in temperature; otherwise, natural aging would be too long [3].

It's now interesting to give more info about the material used in the 2021 season: the AlSi10Mg 2.3. These values were certified by the design partner and supplier at the time: Prima Additive.

Properties	Values
Tensile strength	460 (XY) / 460 (Z) [MPa]
Yield strength	270 (XY) / 270 (Z) [MPa]
Young modulus	75 (XY)/ 70 (Z) [GPa]
Elongation at break	8 [%]
Density	2.65 [ $g/cm^3$ ]
Hardness	55 [HRB]

**Table 2.2:** AlSi10Mg's mechanical characteristics.

As said before these values are subjected to errors, in particular, the materials used for additive manufacturing because they came from powder. Indeed other parameters should be checked such as:

Properties	Values
Particle size distribution	20-63 [ $\mu m$ ]
Thinnest wall	0.3-0.4 [mm]
Layer thickness	30 [ $\mu m$ ]
Roughness	6-10 $R_a$ [ $\mu m$ ]

**Table 2.3:** Additional AlSi10Mg's characteristics.

We will later go more in-depth with these parameters and how they affect the design and the results. Also, it is important to let you know that a tensile test was carried out in the 2021 season. This is crucial for design purposes because, as we can see, the parameters influence not only the strength but even the isotropy of the material.

Three specimens were designed and tested following **EN 10002-1:2001** with the following results:

We can notice similar values concerning 2.2 but with smaller strength; this enhanced the argument discussed before materials data needs to be taken into consideration with proper accuracy values.

<b>Properties</b>	<b>Values</b>
Tensile strength	433 [MPa]
Yield strength	256 [MPa]
Young modulus	71.5 [GPa]
Elongation at break	9 [%]

**Table 2.4:** Specimen’s mechanical characteristics.

## 2.2.2 Component characteristics

The uprights designed in the 2022 season are still mounted on the SC24, thanks to the good design and the right choices in the production process and material selection. The scope of this thesis is to carry out a study on the possible benefits of replacing this component with one produced using additive manufacturing.

The idea is to keep the same interfaces with other components, which are:

**⚡ Suspension geometry**

**⚡ Transmission layout**

**⚡ Brake caliper mounting**

**⚡ Electric motor cooling**

**⚡ Set up angle control**

The suspension geometry, meaning the inner and the outer pick-up points in this study, will be the same as the SC24. It is mandatory to have a fair comparison with the upright mounted on the car, not to mention that studying a new geometry for the suspension is too demanding and out of the scope of this work. Moreover, the suspension geometry is the main constraint of an upright since it needs to fit with all the suspension arms and connect all the other components at the hub and the wheel; thus, comparing two uprights with different pick-up points would be too unfair.

The second interface that must not be changed is the inner part of the upright, which is in contact with the transmission. In particular, the upright is in charge

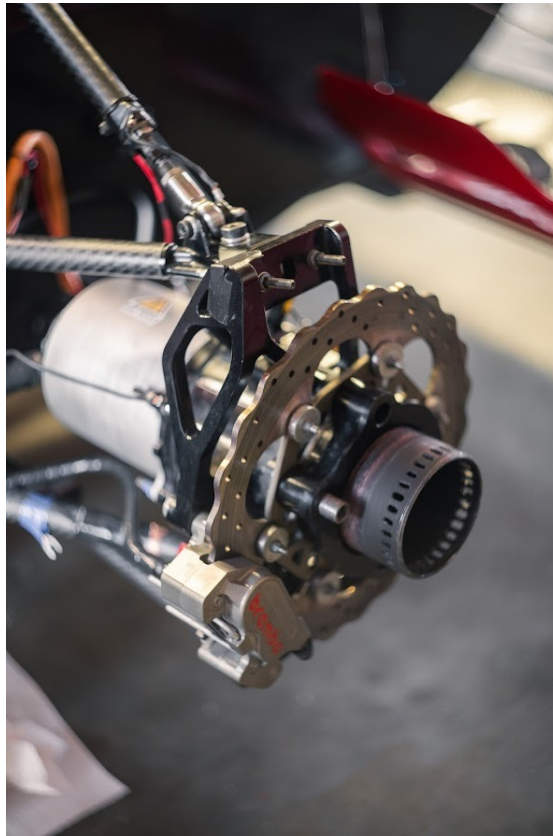


**Figure 2.4:** SC24 wheel assembly: we can see the upright, the suspension arms, the brake system made by caliper and disk, the e-motor, and the hub.

of withstanding loads of the wheel bearings and providing support for the ring gear that is fixed to the upright itself (2.5). This means that the inner part of the upright is filled with oil to guarantee the proper life and functioning of the transmission. From the hub side, which is also the rim side, an oil seal is present, whereas from the electric motor side, a custom motor plate is present with two O-rings placed on the two components' sides. The motor plate is fixed to the motor, and six M5 screws connect the upright to the motor cooling jacket, which is press-fitted on the motor too. Therefore, both the motor plate and the connection mechanism must not be changed.

The last part that must not change is the connection with the brake caliper. This component is fixed to the uprights with two M7 screws instead of the two shoulder screws as said in the 2.1. The distance between the holes is fixed, and the axial direction is set. The axial-type caliper was chosen above all for practical reasons because it's easier to install a proper positive locking system in this configuration. As can be seen in 2.4, the connection is parallel to the axis of the transmission.



**Figure 2.5:** Upright's inner part with only the ring gear, the hub, and the bearing with its oil seal (cannot be seen from this angle). In the front are the holes and the face that connect the motor plate.

Ultimately, it's interesting to point out that the camber can be easily changed by adding or subtracting aluminum shims with proper thickness between the outer upper control arm bracket and the upright itself. Another set-up angle variation is achieved by changing or flipping a component called the flip-chip, which is designed to connect the tie rod to the upright, changing the Ackermann angle (2.6).

### 2.3 Why additive manufacturing?

Additive manufacturing is no longer just a sophisticated process reserved for high-end applications. It has evolved into a widespread technology that enhances component performance and, in some cases, reduces production costs. This is achieved by simplifying tasks that would traditionally require multiple steps into a single operation.

The process proves most advantageous compared to traditional methods when production volumes are low, typically no more than a few dozen units, as is common in prototype development.



**Figure 2.6:** A flip-chip mounted on the upright, we can see the loop shape of the component.

For this reason, in a field like Formula Student, and particularly with complex components such as the upright, additive manufacturing remains highly competitive. Despite the challenges and mistakes encountered in 2021, we have the opportunity to improve our design process and harness the benefits of this technology.

Lastly, I made efforts to further optimize the upright by reducing weight without sacrificing stiffness and strength. However, the performance gains were minimal about the cost. This led me to explore another process, forming the basis of this thesis, to achieve better results than the previous design.

# Chapter 3

## Design targets

In the next chapters, we will dive into the component design. We explain the scope and the need for this work; we can focus on the development process that will lead to the expected result.

It's interesting to have an overview of the steps needed to achieve the best possible component, which will not only perform but also satisfy the targets.

The following diagram 3.1 represents the main steps needed for general component design. In the next chapter, we will see some of these steps in more detail, i.e., the topological optimization and the 3D printing analysis.

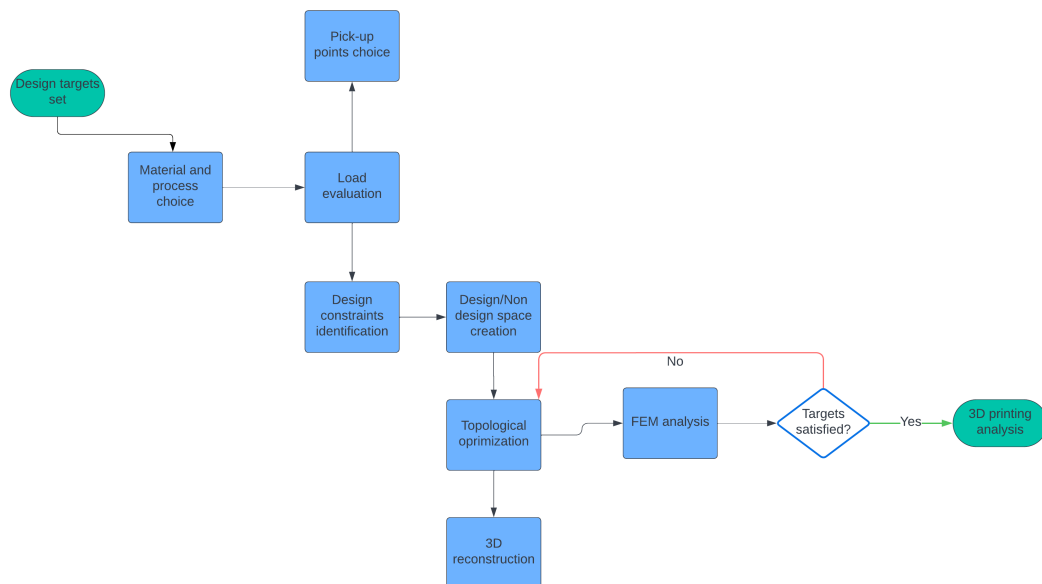


Figure 3.1: Flowchart design steps.

In our case study, some of these steps are already defined: material and process, hard points, and loads.

Now, we will analyze in more detail the targets that need to be achieved to design an upright.

### 3.1 Stiffness

One of the characteristics that is often underestimated in a mechanical component is stiffness. Usually, the weight (and inertia for the rotating part) is the most straightforward parameter used for comparison or to express a component's performance. The stiffness of a component cannot be determined by a single number, as for a simpler element like the spring. Thus, using the stiffness method, we can give a more comprehensive definition.

The stiffness method considers a structure made by nodes, at which we can apply a force or measure a certain displacement. This method is, therefore, written using matrix formalism. Given two vectors in the form of:

$$F = \begin{pmatrix} F_{x,1} \\ F_{y,1} \\ F_{z,1} \\ F_{x,2} \\ \vdots \\ F_{x,n} \\ F_{y,n} \\ F_{z,n} \end{pmatrix} \delta = \begin{pmatrix} u_1 \\ v_1 \\ w_1 \\ u_2 \\ \vdots \\ u_n \\ v_n \\ w_n \end{pmatrix} \quad (3.1)$$

Where the suffix represents the nodes and the algebraic suffix relates to the direction of the force concerning a random set of axes x, y, and z. Thus, we can correlate the nodal force with the nodal displacement to a nodal parameter, which is stiffness, assuming that we are talking about isotropic elements. We can now write:

$$\{F\} = [K]\{\delta\} \quad (3.2)$$

So, we can define the stiffness matrix as:

$$\begin{bmatrix} k_{11} & k_{12} & \dots & k_{1n} \\ k_{21} & k_{22} & \dots & k_{2n} \\ \vdots & \vdots & \ddots & \vdots \\ k_{n1} & k_{n2} & \dots & k_{nn} \end{bmatrix} \quad (3.3)$$

The stiffness matrix is always symmetric but is also singular, and its inverse does not exist, meaning that without proper external conditions on displacements, the relative set of equations cannot be solved.

We can now introduce another concept that will be useful later in this work: compliance. Compliance is the reciprocal of stiffness and in a structure, it can be computed as:

$$C = \frac{1}{2}\delta^T F \quad (3.4)$$

From 3.4 and 3.2 we have:

$$C = \frac{1}{2}\delta^T K \delta = \frac{1}{2} \int \epsilon^T \sigma dV \quad (3.5)$$

Where  $\epsilon$  is the strain,  $\sigma$  the stress, and  $V$  represents the entire volume

This relationship comes from the principle of virtual work (PVW), which assesses the equivalence between the work done by the external forces and the internal work of the system [4]. If we consider a structure with an applied force from 3.2, we have:

$$C = \frac{\delta^T \delta}{2[K]} = \frac{\delta^2}{2[K]} \quad (3.6)$$

Where  $\frac{\delta^2}{2}$  is a constant. Compliance calculation is important for the topology optimization that will be presented later.

Given the basic relationships, now we need to model the structural members. We take into consideration a 1-D rod-type element; it will have two nodes and only translational displacements. This kind of element will have a stiffness matrix of the type:

$$[K]_{rod} = \frac{EA}{L} \begin{bmatrix} 1 & -1 \\ -1 & 1 \end{bmatrix} \quad (3.7)$$

Where  $E$  is the Young modulus of the material,  $A$  is the cross-section resistance, and  $L$  is the length. A more complex type of 1-D element (2 nodes) is the beam, which can withstand any type of load. The stiffness matrix of a beam element subjected to tension, shear, and bending will be:

$$[K]_{beam} = EI \begin{bmatrix} 12/L^3 & -6/L^2 & -12/L^3 & -6/L^2 \\ -6/L^2 & 4/L & 6/L^2 & 2/L \\ -12/L^3 & 6/L^2 & 12/L^3 & 6/L^2 \\ -6/L^2 & 2/L & 6/L^2 & 4/L \end{bmatrix} \quad (3.8)$$

$I$  is the geometrical inertia of the cross-section. For example, the most complete 1-D beam element is represented by a 12x12 matrix. The matrices 3.7 and 3.8 are written in a local reference plane, but to be useful, they must be referred to a global reference system. In this way, we can write a complete structure's stiffness matrix by superimposing the single-element stiffness matrices. In addition, the stiffness

matrix of 2-D and 3-D elements can also be written, enabling the possibility of discretizing real components.

Indeed, this method is at the foundation of the FEM because it can be easily employed in a computer program that can discretize the system into nodes. Each node can be connected to others, forming different types of elements; this process is called meshing. In every single element, we can write the 3.2 and, in particular, the stiffness matrix of the element and solve the system to acquire the displacements, knowing the external loads and constraints. After obtaining the displacements, a series of system equations are solved to get the element's stress and strain. Then this process is iterated for every element. Further explanation can be found in: [5].

This brief introduction to the FEM method and stiffness problem was done to point out that: *the stiffness of a component cannot be precisely computed using analytic computation.* Although we cannot express the stiffness matrix of a component as the upright, we can see in 3.8 that some parameters are common to each element, which are the Young modulus, the geometric inertial, and the length. This underscores *the significance of both material selection and positioning over merely increasing material quantity to enhance stiffness.* Additive manufacturing is competitive in this aspect with respect to traditional processes. Ultimately, FEA will be employed in this thesis, and a basic understanding of these concepts will aid in assessing the reliability of the results.

### 3.1.1 Stiffness targets

After understanding what stiffness is and how it can be computed, we need to pick a certain value to assess if the upright is stiff enough for our application. This is not a simple matter because, as we have seen, a single number is not enough to represent a 3D component. In addition, we need to consider that the upright is connected to the suspension, which is a component that is not still, resulting in a continuous movement of the two, following a path that is a combination of translation and rotation around different axes. This means that the forces exchanged between the two systems change the angle continuously, resulting in a variation of the stiffness (the inertia and length change).

Considering the real operating condition, it seems pretty hard to give a quantification on stiffness, but to figure out a solution, we can question what should be the role of the upright. The suspension system in a race car must [6]:

- ⚡ Maintaining the wheel at the optimum angle with the ground as much as possible**
- ⚡ Keeping the tire in contact with the road surface as much as possible**
- ⚡ Distributing the loads from the tire to the chassis**

The first point is crucial for optimizing the performance. The suspension geometry is designed to exploit the maximum amount of grip from the tires, meaning having the best combination of longitudinal load and tire contact patch dimension. Thus, the position of the outer pick-up points is fundamental and must not change as far as possible to keep the same camber, toe, and caster.

Therefore, a way to express the stiffness of the upright should be the variation of the wheel angles concerning the different load conditions. What matters is how much the outer hardpoints shift concerning the static condition, which is assumed optimal.

$\Delta$ Camber [deg]	$\Delta$ Toe [deg]
$\pm 0.3$	$\pm 0.3$

**Table 3.1:** Maximum variation of the wheel angles allowed by design choice.

Referring to the variation of the wheel angles to the different load cases can be a good starting point to solve the problem. But a load case is a particular condition that can represent the car's performance in terms of acceleration and speed. Thus, to a certain load case, a set of forces, exchanged between the ground and the tires, are computed, and we will see better in 3.2.

This means that the variation can be expressed in terms of degrees, which, in strict terms, is not proper stiffness measurements. Therefore, the next logical step is to refer the wheel angles' variation to forces and moments in different directions. In this way, the actual force's value is not relevant because it is linked to the correspondent angle variation.

Considering that the maximum force exchanged between the tire and the wheel is approximately 3000 N, we can get the values in 3.2

$\Delta$ Camber [deg/kN]	$\Delta$ Toe [deg/kN]
$\pm 0.1$	$\pm 0.1$

**Table 3.2:** Allowed variation of wheel angle with respect to  $F_x, F_y, F_z$ .

The values in 3.2 apply to the entire wheel assembly. The forces at the contact patch are transmitted to the chassis through the hub, upright, and suspension. This sequence of components acts like a series of springs, each with its own stiffness, resulting in a cumulative effect. Since these components are in series, the stiffness of the assembly is constrained by its least stiff component. In other words, even if we increase the stiffness of a single part, the overall displacement will still depend on the most compliant component.

Now, we need to obtain the upright targets only from the values in 3.2, which

refers to the complete assembly of the wheel. Taking advantage of the studies during the design phase, we have the values of the single components; thus, we can extract a reasonable target.

Loads	$\Delta$ Camber upright [deg/kN]	$\Delta$ Toe upright [deg/kN]
$F_x$	0.0013	-0.0145
$F_y$	0.0039	0.0049
$F_z$	0.002	0.0014

**Table 3.3:** Variations of characteristics angle concerning the forces due to the upright in the SC24.

Loads	$\Delta$ Camber wheel ass. [deg/kN]	$\Delta$ Toe wheel ass.[deg/kN]
$F_x$	0.0106	-0.1758
$F_y$	0.042	0.1052
$F_z$	0.0086	0.0032

**Table 3.4:** Variations of characteristics angle concerning the forces of the complete wheel assembly in the SC24.

As we can see in 3.3 and 3.4, the contribution of the upright on the complete assembly is around 10 %. So we can set the following targets.

As our goal is to cover the structural design of the upright, the value of maximum variation is an input given by the vehicle dynamic division, and we will not give more detail about the choice of these values.

It's interesting to note two facts. The first one is that the variations of toe angle are usually more important; this is what we would expect. Sadly, toe angle is usually more critical with respect to the camber because it affects the steering motion. In fact, during the set-up of the car, measuring and putting the right amount of toe angle is very crucial for the performance; in addition, set-up variations are often smaller due to the higher sensitivity to the performance.

The second fact is that the 10% variation can be lower concerning the expected values; considering the upright as the biggest component in the wheel assembly, we would have said that it was the most compliant component. The results show that the biggest compliance is introduced by the chassis panel, which is bigger and has a young modulus similar to the aluminum one. This can be explained in part by a non-validated FEM model used to get this result and in part by the fact that the material used is not as stiff as it should be. Ultimately, it should be said that even the suspension systems are more compliant than the upright; this is due to the presence of the aluminum insert that reduces the stiffness of the carbon tubes.

$\Delta$ Camber [deg/kN]	$\Delta$ Toe [deg/kN]
$\pm 0.01$	$\pm 0.01$

**Table 3.5:** Upright contribution of the allowed variation of wheel angle concerning  $F_x, F_y, F_z$ .

## 3.2 Reliability

For a mechanical component, being able to withstand all the load cycles without failing is clearly the number one requirement. First of all, a specification must be made; we will discuss the static safety factor targets. A fatigue study will be conducted, but not with a proper target due to the lack of know-how to establish one. We recall that as a safety factor, we mean:

$$SF = \frac{\sigma_{yield}}{\sigma_{max}} \quad (3.9)$$

We have already discussed the yield strength of the material in 2.2, and 3.9 explains why the safety factor, which is the main indication of reliability, is greatly influenced by the yield strength of the material. Thus, reducing the target safety factor without being positive about the material characteristics can be dangerous.

Moreover, the safety factor depends also on the maximum (Von Mises) stress. To compute this value, we use the FEM method that we will see in the next chapter. The FEM method is introducing a certain amount of error that is difficult to estimate. We need to remember that FEM is just a model of reality and more than often cannot reproduce exactly the operating condition, especially of a component complex as the upright. The FEM model, indeed, is a static evaluation, whereas the upright is a moving object and, at the same time, is influenced by different systems such as suspension, brake, and transmission. For practical reasons, it is impossible to simulate a complete assembly because the amount of meshing elements would be too high, and thus, the computational effort is too demanding.

The solution here is just being on the safe side, increasing the safety factor targets, and trying to overestimate the model. This is not the best practice in terms of performance; nevertheless, the amount of mass that we can subtract is on the order of tenths of kilos, whereas a component failure could potentially end the season. Thus, seeing the problem from this perspective, we can safely say which is the right approach.

### 3.2.1 Reliability target

Now that we have given the definition of reliability and made some considerations, we can set the target for this work. *The suggested safety factor for a motorsport*

*application is 2*, as said in [6]. In this application, though, the uncertainty of the production process, as said in the previous chapter, needs to be taken into consideration by adding another factor of 1.25. This factor is arbitrary and comes from a mix of experience and some advice from expert professionals. Thus, the real safety factor is:

$$SF = SF_{literature} * SF_{process} = 2.5 \quad (3.10)$$

Also, a coefficient taking into account the uncertainty of the loads during the working condition should be applied. But if we consider the fact that the same loads were used to design the SC22 uprights, we can neglect them, since after thousands of kilometers, the upright did not have a single problem.

This target is the one used in the design phase and needs to be respected only on the load cases that are intentionally used for design purposes. We can introduce other load conditions more severe, which must be used only for verification scope. These conditions should not have a proper safety factor target, but they need only to be verified as having 3.9 higher than 1.

SF design	SF verification
2.5	1

**Table 3.6:** Reliability targets summary

### 3.3 Weight

Weight is a critical performance factor, especially for race cars. In all motorsport disciplines, minimizing weight is one of the most straightforward ways to improve lap times. However, the topic becomes even more essential when discussing unsprung masses. Because of their distance from the car’s center of gravity, these masses significantly impact the vehicle’s yaw moment of inertia, which opposes cornering speed. Simply put, a car’s resistance to rotation during a turn is directly influenced by the positioning and the weight of these masses relative to the center of gravity.

When it comes to a component like the upright, this topic becomes complex. As noted at the end of 3.2, in this project, we prioritize stiffness and reliability over raw performance. Nevertheless, the upright, being the largest component in the wheel assembly (aside from the rim, which is not designed by our team), has the greatest impact on the assembly. Therefore, by the end of this study, it will be crucial to understand how additive manufacturing can be exploited to increase stiffness while maintaining or reducing the weight, keeping both stiffness and reliability at an acceptable target.

### 3.3.1 Weight targets

The target set is to keep the same weight as the upright of the SC22. This seems acceptable because the actual stiffness targets imposed in this study are stricter than the ones of the 2022 season.

SC22 front upright weight [g]	SC21 front upright weight [g]
895	719

**Table 3.7:** SC22 and SC21 upright front weight

# Chapter 4

## Component design

In the following chapter, we are going to discuss the loads on the component. The first step is to identify which are the design load cases and the verification ones. The next step is to explain how these loads are applied to the upright to come up with the stresses and the displacements.

We will not see yet the FE models because there will be a dedicated chapter, but we figure out which are the input models of the FE software.

### 4.1 Load cases

Knowing the loads a component can withstand during its life cycle is crucial for structural design. A component like the uprights is very difficult to address because it's directly linked with the forces exchanged between the tire and the ground. Thus, the proper way to handle this problem should be via a proper load spectrum that comes from the direct measurement during a road test.

Therefore, the approach used during this work is based on the load cases. Practically, the maximum performance of the vehicle is determined in the different areas like braking, acceleration, lateral, and combined. An acceleration and a velocity are set for each of these cases; in this way, all the forces between the tire and the ground can be computed. We will not see the complete procedure because, as we said, the main focus of this work is the structural design.

Setting the maximum performance means verifying the safety factor under the worst possible *operating condition*. We must stress these words because we focus on the design steps. In this phase, we cannot take into consideration extreme load conditions, such as coming through a bump. For this reason, we set different safety factors in 3.6; otherwise, using an extreme condition in the design phase can lead to an over-dimensioning of the component.

### 4.1.1 Design load cases

The following load cases will be used for the design:

Load cases	$\mathbf{a}_x$ [g]	$\mathbf{a}_y$ [g]	$\mathbf{F}_x$ [N]	$\mathbf{F}_y$ [N]	$\mathbf{F}_z$ [N]
<b>PB</b>	-3	/	2781	/	1885
<b>PL</b>	/	2.5	/	2760	1714
<b>BIT</b>	-1	1.5	1148	1721	1504

**Table 4.1:** Input data for the design load cases for the front upright

The adopted car reference system has the x-axis pointed to the rear of the car, whereas the y-axis is pointed to the right (seeing the vehicle from above), and the z-axis follows the right-hand rule. Thus explaining the sign of the forces and accelerations.

As suggested in [6], the upright should be dimensioned on the braking and lateral cases. In addition, a combined case should also be defined to see what happens when both loads are present. The acceleration case is more demanding for the rear upright, being in some way the opposite of the front for braking.

Moreover, a point, which represents the contact patch, is given by the vehicle dynamic division; here, it is not reported because it is not interesting as it is but rather important for the FEMs.

### 4.1.2 Verification load cases

In addition to the previous load cases, verifying the components under more severe conditions is interesting. During the vehicle's life, it can happen on track to face uneven road surfaces or particularly high curbs. These obstacles can generate an impulsive force due to the sudden increase in vertical and longitudinal accelerations produced by overcoming them, which is not considered in the design case.

The proper treatment of this condition should include a complete multibody suspension model, which can accurately represent the accelerations and forces on the individual components. The vehicle dynamics division develops this model, but further study can be conducted to implement the model in FE software that can output stresses and displacements.

Thus, we decided to implement a load case called *bump*, which is defined by an input velocity and a consequential vertical acceleration. This will add vertical and longitudinal forces to the design load cases. The design load case is already defined

by a particular velocity, so in case they don't match the design case, a simple linear interpolation is performed.

Load case	$F_z$ [N]	$F_x$ [N]
<b>PB</b>	7473	4133
<b>PL</b>	5840	3367
<b>BIT</b>	4240	2600

**Table 4.2:** Bump load case input force to be added to the design load case

Referring to 4.1, we can add the values of 4.2 and find the new input forces.

The difference between design and verification is the safety factor choice. For the latter case, we do not define a safety factor, but the idea is to verify if the stress in the component is less than the material's yield strength. The point is that the input loads are quite significant, and it is very difficult to face these conditions during the vehicle's life.

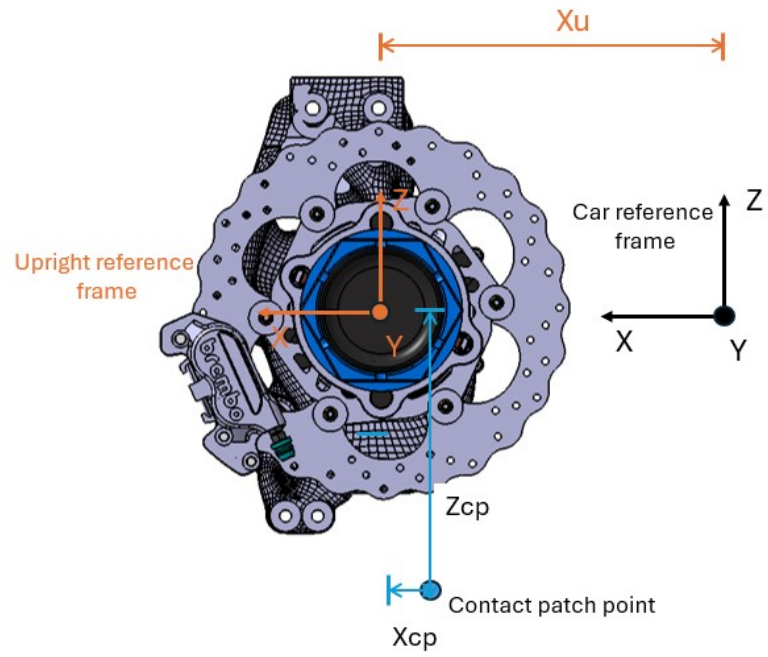
## 4.2 Loads model

In the following chapter, we are going to discuss how the loads from the contact patch are distributed on the upright. The free-body diagram changes with the different load cases, but the main idea is to transfer the forces from the contact patch point to a made-up point called the *bearing's center*; thus, we need to apply transport moments to the structure to balance it [7].

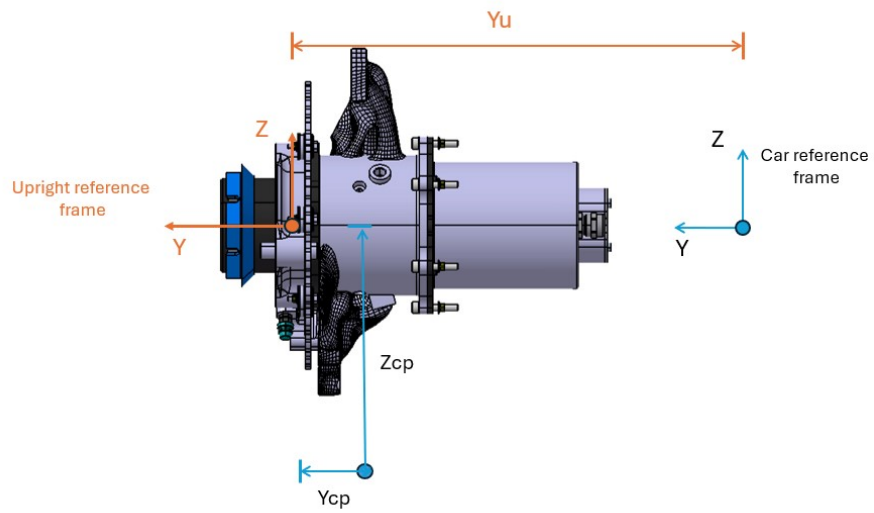
Starting from the forces and the coordinates of the main points, which are the contact patch, the bearing center, and the upright center reference frame. The latter point is, similar to the bearing center, an arbitrary point used to simplify the computation, transporting every geometrical element in a more convenient reference frame. The point is chosen on the external surface of the upright and aligned with the wheel center.

$$\begin{cases} x_{cp} = X_{cp} - X_u \\ y_{cp} = Y_{cp} - Y_u \\ z_{cp} = Z_{cp} - Z_u \end{cases} \quad (4.1)$$

Where  $x_{cp}$  is the contact patch coordinate expressed in the upright reference frame,  $X_{cp}$  is the coordinate of the contact patch expressed in the car reference frame, and  $X_u$  is the center of the upright reference frame expressed in the car reference frame.



(a) XZ plane upright and car reference frames



(b) YZ plane upright and car reference frame

**Figure 4.1:** Upright reference frame and car reference frame

In doing so, we compute the distance between the coordinates of the contact patch and the bearing center. Shifting the loads to the bearing center, we need those distances because, multiplied by the loads, we obtain the transport moments. For each load case, we compute the transport moments in the three directions using the following equations.

$$\begin{cases} M_x = |y_{bc} - y_{cp}| |F_z| + |z_{bc} - z_{cp}| |F_y| \\ M_y = |x_{bc} - x_{cp}| |F_z| + |z_{bc} - z_{cp}| |F_x| \\ M_z = |x_{bc} - x_{cp}| |F_y| + |y_{bc} - y_{cp}| |F_x| \end{cases} \quad (4.2)$$

Where  $x_{bc}$  represents the bearing center coordinates in the upright reference frame. The absolute value is used because the sign is adopted according to the clockwise convention and is determined using a *control if* in the code.

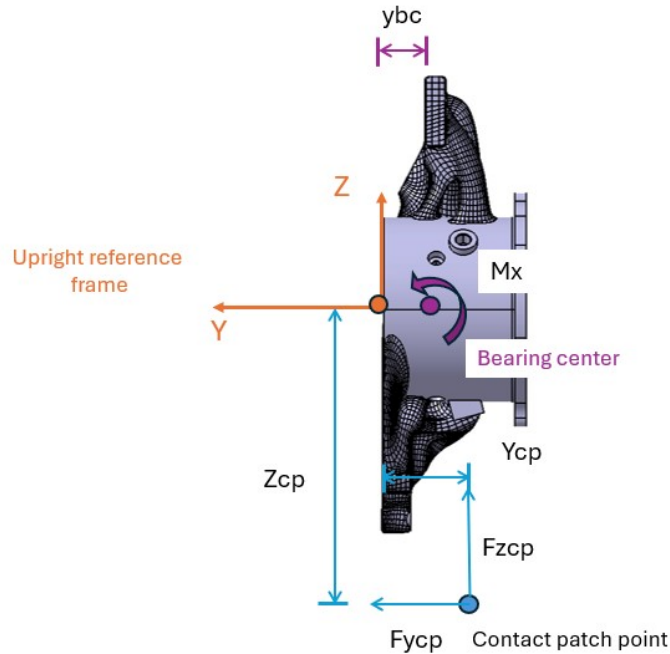


**Figure 4.2:** Mx transport moment computation example

Whereas in the braking load cases, the values found in the 4.2 are a little bit different because we need to take into account the contribution of the brake caliper forces.

Thus, the product of the longitudinal force is not involved in the My value, but we apply the force due to the brake caliper positioned at a distance equal to the mean radius of the brake disk. So, we need to add a proper transport moment to

the bearing center where the distance is between the brake caliper force application point and the bearing center.

In this case, the braking torque contribution due to the longitudinal force is already accounted for in the caliper force, so we should not add it twice. The computations are a little bit more difficult because the brake caliper has a slope  $\alpha$  relative to the vertical direction. This will lead to a double component force along x and z and a related transport moment, as we can see in 4.3.

$$\begin{cases} F_{x_{cal}} = \frac{F_z z_{cp} \sin \alpha}{R_{cal}} \\ F_{z_{cal}} = \frac{F_x z_{cp} \cos \alpha}{R_{cal}} \\ M_{x_{disk}} = F_{x_{cal}} |y_{cal} - y_{bc}| \\ M_{z_{disk}} = F_{z_{cal}} |y_{cal} - y_{bc}| \end{cases} \quad (4.3)$$

Where  $R_{cal}$  is the mean value of the brake disk radius and  $y_{cal}$  is the coordinate of the application point of the caliper force.

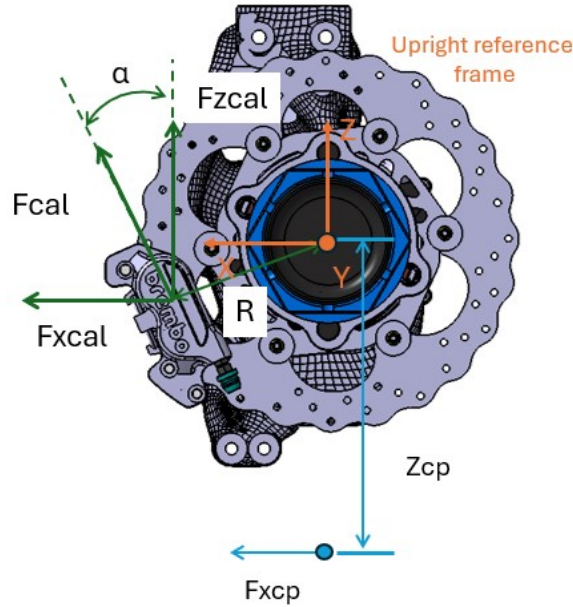


**Figure 4.3:** Brake loads computation example

Lastly, in the acceleration case, we have to add the contribution of the motor plate, which is joined to the upright as said before, computed as:

$$M_{mp} = \frac{M_y}{\tau} \quad (4.4)$$

Where  $\tau$  is the transmission ratio.

<b>Loads</b>	<b>PB</b>	<b>PL</b>	<b>BIT</b>
$M_x$ [Nm]	-39.5	522	325
$M_y$ [Nm]	20.3	14.2	78.7
$M_z$ [Nm]	58.3	-22.8	20.3
$M_{xdisk}$ [Nm]	300	/	124
$M_{zdisk}$ [Nm]	-134	/	-55.2
$F_{xcal}$ [N]	-2846	/	-1174
$F_{zcal}$ [N]	-6386	/	-2638

**Table 4.3:** Summary of all the computed loads for the front upright

## 4.3 Fatigue study

In the following chapter, we will discuss the model used to assess the fatigue life of the component.

Fatigue is a dynamic phenomenon, and it is based on statistical studies on the possibility of failure after a large number of load cycles. For the application and the lack of time and instruments, we could not make a proper study campaign to get a realistic target or a normalized load cycle. A race car is always dealing with different types of stresses and transient conditions.

Nevertheless, as we have seen in the previous seasons, a failure at a low number of cycles happened, and we could not neglect it. Thus, trying to develop a fatigue study and perform a fatigue analysis can show us a different type of defect in the design of the component that can lead to problems.

### 4.3.1 Fatigue load case

Some assumptions are made:

- ✍* Fatigue loads are in the elastic field of the material and the case of the high number of cycle
- ✍* The type of damage on the component is linear and cumulative
- ✍* The load case is constructed as a sum of static load cases one after another

The first two assumptions deal with the model used to simulate the fatigue problem. They allow us to use the most basic fatigue model to avoid difficult simulation and obscure results analysis. The last assumption is made due to the impossibility of elaborating a precise fatigue load case due to the dynamic nature of the problem. Considering what is needed as an input for the load cases, we would need to compute the coordinate of the contact patch at each single time instant after computing the loads between the tire and the ground. It's becoming clear that it's quite computationally heavy.

Starting from test data collected at the Cerrina Race Track, we were able to obtain the acceleration, velocity, and position of the car. The data are coming from an autocross run, which is the single lap when the driver pushes the car next to the limit, and likely the exchanged loads and power are the highest. Thanks to the model of the car and the tire, the vehicle dynamic division was able to compute the forces at every instant. In this way, there is one input, but we lack the contact patch coordinates. As said, the third assumption was made to make up for that. The idea is to establish a connection between the static condition and the instantaneous dynamic condition of the car.

To determine which load case condition is the most suitable to represent a specific instant, the ratio between the lateral force and the longitudinal force is computed. If this ratio is significantly lower than one, we end up in a pure braking or pure acceleration load case. If the ratio is about one, we are in a combined load case, and if the ratio is larger than one, we are in a pure cornering condition.

At this point, we have the loads and the coordinates of the contact patch, and we can compute every reaction seen in 4.2. The results are normalized concerning the static load of the correspondent load case; this is done to satisfy the request of the analysis software.

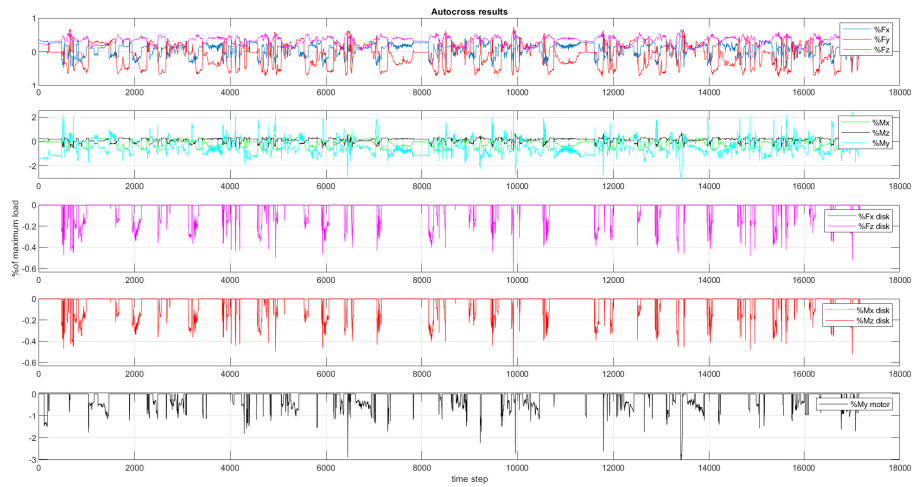


**Figure 4.4:** Reaction on the upright of a simulated autocross lap

We can note that in 4.4, the normalized contribution of the disk reactions is the same. This is because the sine and cosine are canceling out with the ones of the static condition.

# Chapter 5

## FEM models

In the following chapter, we discuss the finite element models needed to output the target parameters explained in the chapter 3. To find stiffness and reliability targets, two different models must be developed starting from the same input forces discussed in the chapter 4. Both models were developed using Altair software, Hypermesh. The solver exploited is Optistruct, which is common for structural applications.

Moreover, we implement another finite element method called *topology optimization* to find the best trade-off among the fixed targets. This analysis will be performed using Inspire software (the same solver), which is more straightforward for this application. After performing the optimization, we reconstruct the 3D file, and through the models mentioned above, we will find out if the design is compliant or not. Otherwise, as explained in 3.1, we will perform the analysis again or change the material.

The topology optimization and the structural analysis models share the same inputs; thus, we will illustrate the FEM first for practical reasons.

### 5.1 FEM model for structural analysis

In the following section, we will discuss the basis of the FEM models to practically understand how these models are built. The FEM is a complex and intense world of structural mechanics; in this work, we are not aiming to fully discuss and understand how the FEM software works and should be used. Nevertheless, after some years of experience and good practice shared among colleagues, we intend to report the basic notions needed to perform a correct analysis.

We already anticipate in 3.1 how the FEM works, but now we can dive a little more into it.

FEM is based, as said, on elements, which are an idealization for a portion of a

physical part [8]. Elements can be 1D, 2D, and 3D. Every physical component must be discretized using the needed element's kind and number. This brings us to the first important concept: accuracy. FEMs are based on models of reality that are not correct by definition; using a 2D or 3D element is not wrong by definition. Only good practices, found through experience and physical testing, can produce a more robust result. A FEM result can be defined as correct if there is a convergence of the error, which is always present because it's just an idealization of reality. Fixed this concept, we can discuss the type of element used in a FEM.

To perform a FEM analysis, we need 1D elements:

**RBE2**: also called Rigids. They connect an independent node named Master to one or more dependent nodes called Slave and are often used to represent rigid bodies or rigid movements.

**RBE3**: connect one or more slave nodes to a master node. It is usually used to link the motion of a dependent node as an average of the independent ones. For this reason, it is preferable to use it with loads.

The upright is modeled using a combined 2D element mesh and a 3D mesh. The 2D element mesh is made of tria and quod elements. Respectively triangular and squared elements.

The mesh is essential because each element introduces a certain shape error that is quantified by different parameters such as jacobian, aspect ratio, skewness, and warpage. An element fails when it does not respect the limits imposed by the user or the software for each one of these parameters. From a failed mesh, it is not possible to run the analysis, or in other cases, the results won't converge. Reducing the element size is an option to solve the problem, but the analysis will take more time. Thus, reducing size is not always the solution, and sometimes, a manual correction of every element is needed.

The 3D mesh works with the same principle. We decided to use the pyramidal elements called tetra to model the 3D shape. A 3D analysis is compulsory when the studied component has three dimensions similar to the upright.

In addition to elements, FEM software needs more input to run the analysis. Every component with a mesh must have a property that gives the basic information to the solver, for example, the material type and the properties of the material.

Ultimately, the boundary conditions need to be set, and we have:

**Loads**: forces and torques that are applied to the structure using RBE3.

**SPC**: single-point constraints block the degrees of freedom of the component. They are applied using RBE2 because the displacements of the master node must be the same as the slave one.

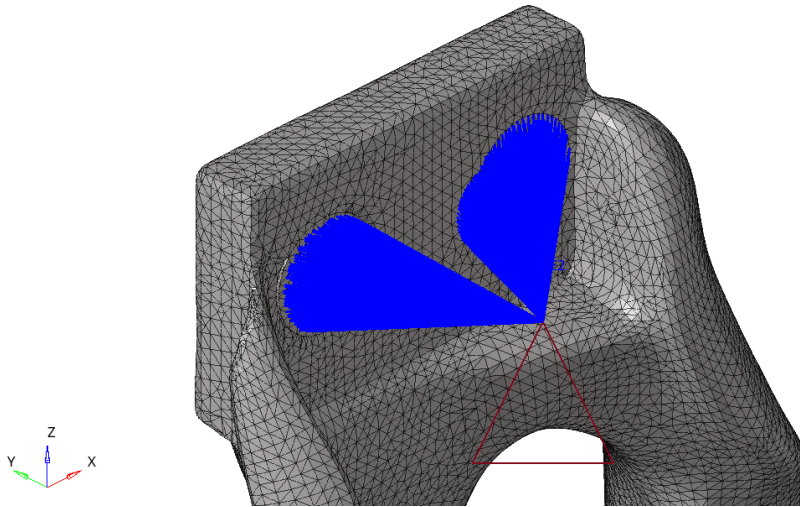


**Figure 5.1:** RBE2 and single point constraint applied in the FEM model

### 5.1.1 Reliability FEM model

Given the basis of the FEM, we can now explain how it is built and use the model for verifying the structural integrity of the upright. The output of this model will be the maximum Von Mises stress of the component.

Starting from the loads explained in Chapter 4, we first mesh the component as discussed above, and secondly, we apply the boundary condition. As said, we have different load cases, but the common loads are:  $F_x$ ,  $F_z$ ,  $M_x$ ,  $M_z$ .

The two forces are applied at the bearing center to the inner surface of the bearing through an RBE3 because they are withstood by those components. The same is done for the two moments. The bearings, indeed, are modeled as two disks, which give the necessary radial stiffness to the component.

The  $F_y$  is applied to the lateral side of the bearing because it is an axial force. The bearings are spherical; thus, they can stand lateral forces, but they are mounted in a "O" configuration, so the loaded bearing depends on the sign of the force. Due to the press-fitting, the bearings are capable of counteracting a certain amount of lateral friction; thus, for the friction, we can consider applying this to the previous ones.

The  $M_y$  is instead applied to the inner edge of the upright's housing, which is rigidly connected to the ring gear. The latter component is, in fact, unable to rotate, as said before; thus, a certain torque is transmitted to the upright, which is exactly the counteraction of the torque useful to accelerate or to brake. As for the sign of the  $F_y$  force, here the idea is the same; it is applied only on the surface side in concordance with the rotation of the torque. This concept is also valid in

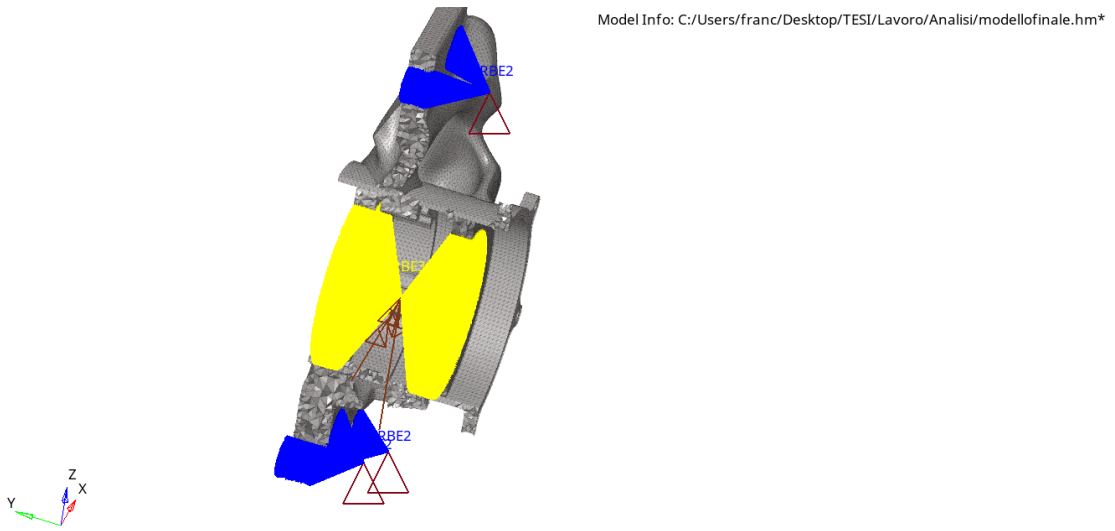


**Figure 5.2:** RBE3 and forces applied to the bearing center in the FEM model

general, and it's worth elaborating on.

It's good practice to apply the connection only to the surface portion that is in contact due to the force direction. In other words, consider the example of a force applied tangentially to a pin inserted into a hole. The only part of the hole subjected to a force is the one opposite to the direction of the force. This consideration should be done every time we apply a force to the component and even when we apply constraints.

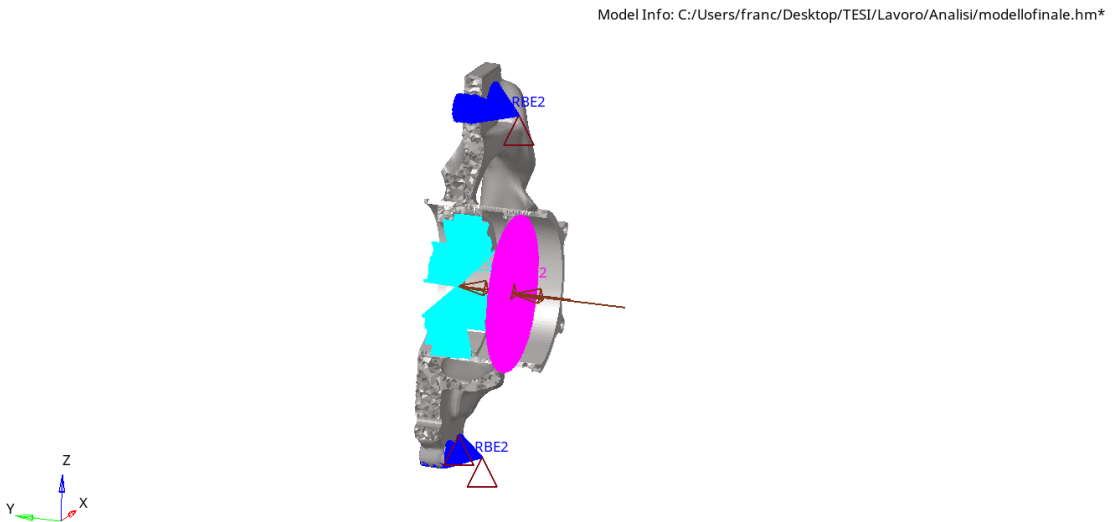


**Figure 5.3:** RBE3 and forces applied in the lateral direction

The motor plate torque presented in the acceleration cases is applied with an RBE3 to the flange surface that connects the motor plate with the upright. Due to the presence of 6 screws, the flange surface is in contact with the motor plate; thus, the friction force is exchanged on this surface.

In braking cases, the force applied to the brake caliper is positioned at the contact between the disk and the pads. An RBE3 links the force with the surface around the two holes used for the brake caliper mounting. As discussed, it is also reported to the bearing center, and in addition, transport moments are applied at the same point.

It's important to apply the RBE3 only around the holes and not inside because the two components are attached through the friction force, distributed on the contact surfaces.

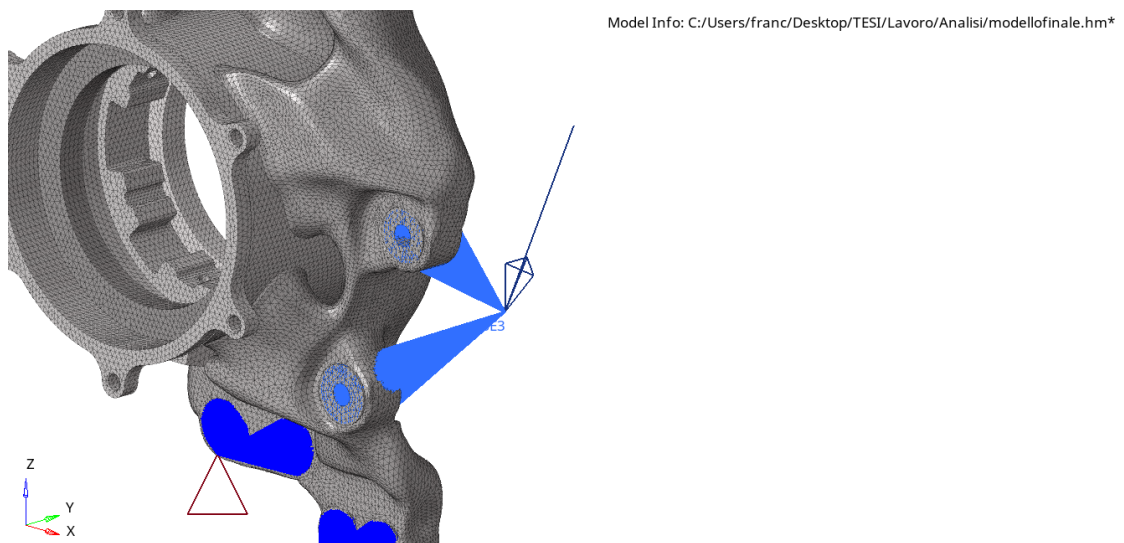


**Figure 5.4:** Caliper forces and RBE3 applied in the FEM model

### 5.1.2 Stiffness FEM model

The most concerning problem with the stiffness model is dealing with the number of components that should be involved in the model.

Using only the upright should be the best solution because, in this way, we are computing only the stiffness of the component. At least, if additional components must be involved, they need to be modeled as orders of magnitude stiffer than the upright. The introduction of the wheel hub and carrier has been mandatory for two reasons. The first one concerns the real upright assembly, which is always mounted on the car with those two components. Different analyses have shown a considerable lack of stiffness without considering the bearings and the hub. Even

the static model shown previously comprehends at least the bearings. The second reason deals with the application of the loads that must be addressed using the hub. In other words, as we explained in 3.1 the stiffness is not influenced by the module of the force; thus, we use as input forces 1000 N in every direction to obtain the results in the three directions. Moreover, the input forces are not internal reactions of the upright with other components, but they are forces exchanged between the tire and ground at the contact patch. Ultimately, the forces are applied to the hub, which is the component fixed to the wheel rim and is in charge of transferring the loads to the components.

Explained the reasons why we need to involve both the hub and the carrier, we will explain how the model is built. The input loads are three 1000 N forces in every direction, applied to the hub with an RBE3 connecting the center of the contact patch to the threaded part of the hub, which is the one where the friction force between the hub and the wheel nut is exchanged. The constraints are different from the reliability model because we need to avoid adding unwanted stiffness to the model. Thus, following the scheme in [6], we fixed the translational degrees of freedom concerning x and y direction for the lower control arm outer point, the same way for the Tie outer hardpoints. The remaining degrees of freedom are fixed in the upper control arm. Freeze-type contact among the components is used to fix everything.

The last part of the model deals with the computation of the characteristics of wheel angle variation. The easiest way would have been considering the variation of coordinates of the outer points; unfortunately, it's not possible because they are constrained in the model. Thus, we can select the coordinates of three non-aligned points belonging to the static plane of the wheel. These points must be fixed with an RBE3 to the upright so that they will have the same displacements of the component. It's important to stress the fact that the RBE3 is the only way to connect an external point to the upright so that the displacements are transferred to points 5.5.

After the analysis, these three points will change their coordinates, lying in a different plane. Considering the new plane coordinate in the frontal and upper view, we can evaluate the difference with respect to camber and toe angle.

<b>Points</b>	<b>X [mm]</b>	<b>Y [mm]</b>	<b>Z [mm]</b>
<b>Wheel center</b>	0	601	0
<b>Wheel system X</b>	100	601	0
<b>Wheel system Z</b>	0	601	100

**Table 5.1:** Coordinates of the three points used to compute the angle variations

Model Info: C:/Users/franc/Desktop/TESI/Lavoro/Analisi/Hypermesh/modellostiffness.hm\*

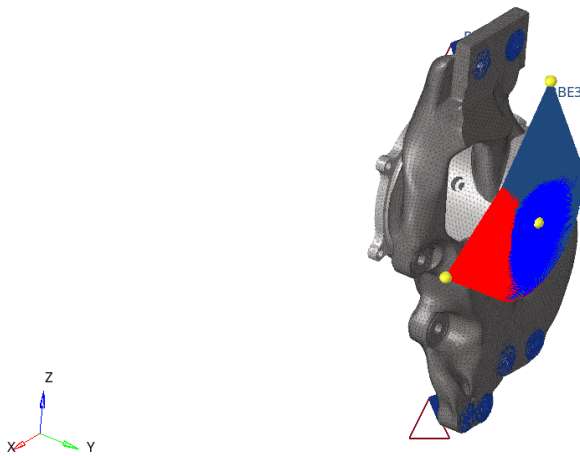


**Figure 5.5:** RBE3 connection between the upright and the point where the displacements are measured

Model Info: C:/Users/franc/Desktop/TESI/Lavoro/Analisi/Hypermesh/modellostiffness.hm\*

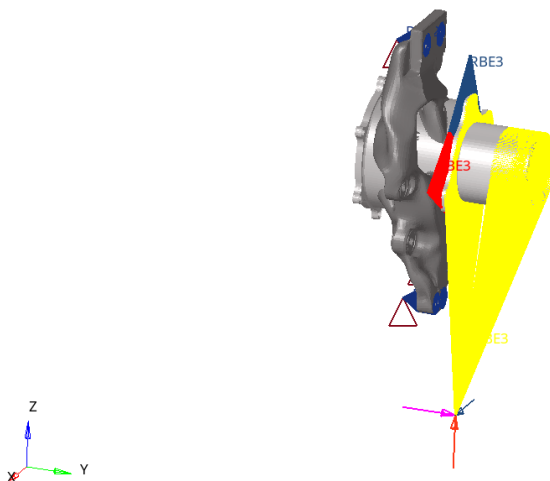


**Figure 5.6:** Stiffness model in Hypermesh

## 5.2 Topology optimization

In the previous chapters and sections, we introduced the foundations of FEM and what are the targets expected from our component. At this point, the process of design is focused on using the material and the space available to find the most suitable configuration. Practically speaking, we need to find the optimum

component's shape that can withstand the loads, provide sufficient stiffness, reduce the weight as much as possible, and keep an eye on cost and producibility.

We can highlight some key concepts: optimum shape, strength, stiffness, weight, and producibility. We need an instrument that can find the optimum shape given certain types of constraints; fortunately, the FEM can help us with the so-called topology optimization.

Topology optimization is a mathematical technique that produces an optimized shape and material distribution for a structure within a given package space. By discretizing the domain into a finite element mesh, OptiStruct calculates material properties for each element. The OptiStruct algorithm alters the material distribution to optimize the user-defined objective under given constraints.

During the optimization, the solver's job is to find a global minimum of an objective function given certain constraints, formalizing:

$$\min(f(x) = f(x_1, x_2, \dots, x_n)) \tag{5.1}$$

subjected to:  $g_j(x) \leq 0$  where  $j = 1, 2, \dots, m$   $x_i^L \leq x_i \leq x_i^U$  where  $i = 1, 2, \dots, n$ .

The selection of the vector of design variables  $x$  depends on the type of optimization performed. In topology optimization, the design variables are the densities of the elements, but other types of optimization can have different design variables.

OptiStruct monitors and plots the design responses, which are properties that can be used as objectives or constraints. Some of these responses can be global, meaning computed on the whole structure, or proper of a single element. In addition, the responses can depend on the loads or not.

Having set the responses that we want, the next step is the selection of the objective function, which, in our case, is compliance minimization. Thus, the software will compute the structural compliance, as seen in 3.1, until the requested constraints are satisfied and the solution has converged.

The software changes the density of the single elements. The design variable in the topology optimization is the element density, which will be the only variable that the software can change. With the density method, the material density of each element is directly used as the design variable and varies continuously between 0 and 1; these represent the states of void and solid, respectively. Intermediate values of density represent fictitious material. The stiffness of the material is assumed to be linearly dependent on the density. This material formulation is consistent with our understanding of common materials. For example, steel, which is denser than aluminum, is stiffer than aluminum.

In general, the optimal solution to problems involves large gray areas of intermediate densities in the structural domain. Such solutions are not meaningful when you are looking for the topology of a given material and not meaningful when considering the use of different materials within the design space. Therefore, techniques need to be introduced to penalize intermediate densities and to force

the final design to be represented by densities of 0 or 1 for each element. The most used one is called Solid Isotropic Material with Penalizations SIMP based on the equation:

$$\bar{K}(\rho) = \rho^p K \quad (5.2)$$

Where,  $\bar{K}$  and  $K$  represent the penalized and the real stiffness matrix of an element, respectively,  $\rho$  is the density, and  $p$  is the penalization factor, which is always greater than 1.

Topology optimization is always more time-consuming than a simple FEM analysis. The reason why is that it's an iterative process, which means that in every step it solves a FEM analysis and computes the design responses. In addition, convergence criteria must be met; this criterion ensures that the minimum found in the objective function is global and not a local one.

### 5.2.1 Topology optimization model

The following steps can be considered to set up a topology:

- ✍ Generate a finite element mesh on the component.
- ✍ Parts of the mesh are designated as **non-design space**.
- ✍ Loads and constraints are applied to the finite element model.
- ✍ The objective response function is established, the proper density of volume elements is decided, and it's called **design space**.
- ✍ The needed constraints are set.
- ✍ The model and parameters are submitted to OptiStruct for topology optimization.

The next logical step is to generate a design using the optimized shape, considering manufacturability and costs.

It is worth pointing out that the non-design space is a part of the component not optimized by the software. The non-design space is the zone where loads and constraints are applied.

A stress constraint is applied to the model to ensure that the highest stress on the material is lower than the desired one.

For what concerns the FEM model, we have the same loads and constraints applied to the upright as in the previous section. There are small differences because we are using different software.

The last important topic that we need to discuss about topologic optimization is manufacturability. After the analysis, we have an optimal shape functionally;

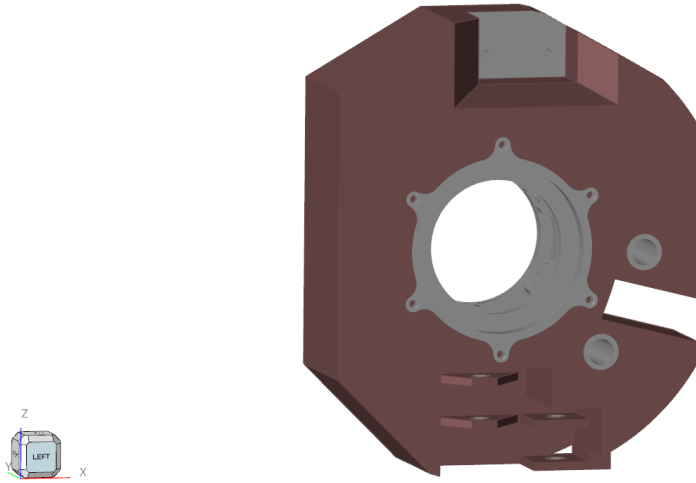


**Figure 5.7:** Starting model for topology optimization, in grey the non-design space and in brick red design space

in other words, the software does not recognize a shape that is difficult or even unfeasible to produce. This is true, especially for traditional production processes; this is the way imposing symmetry and design constraints can help, but it will not solve the problem.

In this case study, we will exploit additive manufacturing, which can reduce some concerns about shape manufacturability, but at the same time, we need to take into consideration the introduction of a constraint called overhang. Due to the characteristics of additive manufacturing, it's important to avoid that all the parts of the component are not supported by a layer of material. The overhang constraint ensures that all the elements of the model do not stick out beyond a certain angle that depends on the material chosen; usually, it is  $45^\circ$ . If this condition is not met, support structures need to be built.

### 5.3 Fatigue analysis

The model used for the fatigue analysis is quite simple. Hypermesh allows you to make a fatigue analysis starting from a FEM model. The most important difference concerning the FEM reliability model is the input loads. In other words, the software expects as input a cycle history of every single load in the model. For this reason, the FEM model must be built with every single internal reaction.

The input load cycle is transmitted as a file built as a 2-column array in which

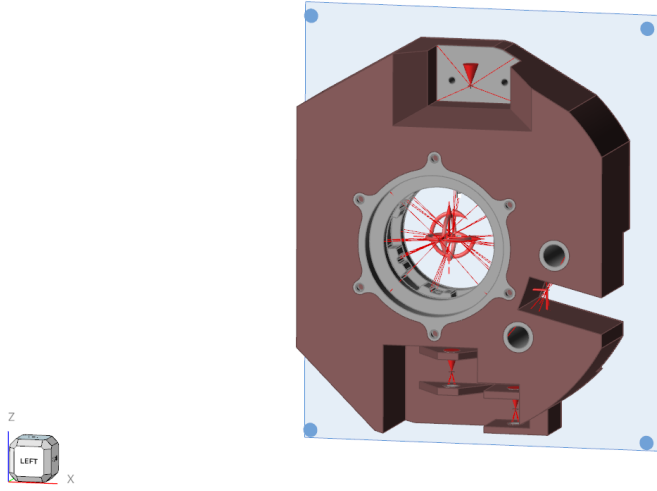


**Figure 5.8:** Optimization model in Inspire. Constraints, loads, and 1-D elements are applied to the gray part, the non-design space. The blue plane is the overhang constraint.

you have in the first column the time step and in the second the ratio between the load at that particular time and the load inserted in the FEM model. The ratio can be higher than 1. As we have seen in 4.4.

The input FEM model is a combination of the different load case models; note that the input FEM model should be run as the fatigue model needs the result of static FEM. Remembering the assumption made in 4.3, the model used to simulate the fatigue life is the uniaxial fatigue. It's used because of its simpler approach, and in the literature, it is the most suggested for the stress-life approach. The stress-life approach is based on the assumption that the component withstands loads only in the elastic range and the number of cycles is high; both are coherent with what has been assumed.

Now, it's interesting to give some insight into how the solver runs a fatigue analysis. It starts with the S-N (stress range-number of cycles) curve, or the Wöhler curve. This diagram is built starting from the material data, and it's supposed to have a mean stress equal to 0. Nevertheless, in real conditions, the mean stress of a cycle is not always 0; thus, a correction is made. Different theoretical models are present in the literature, but the most used for ductile material is the GERBER one, based on the equation:

$$\sigma_e = \frac{\sigma_r}{\left(1 - \left(\frac{\sigma_m}{\sigma_u}\right)^2\right)}. \quad (5.3)$$

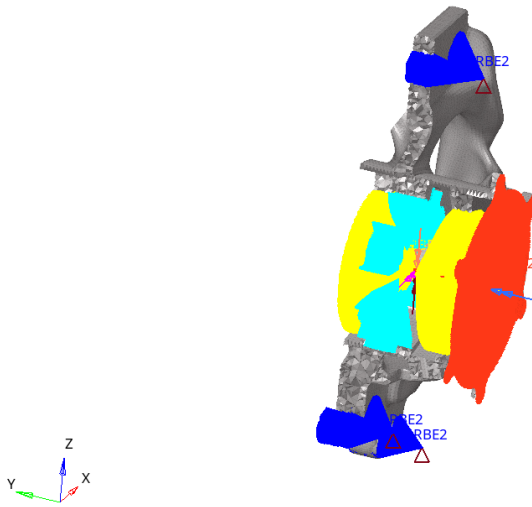


**Figure 5.9:** Fatigue analysis FEM model. All the loads and RBE3 are applied

Where  $\sigma_m$  is the mean stress given by  $\sigma_e = \frac{\sigma_{max} + \sigma_{min}}{2}$ ,  $\sigma_r$  is the stress range given by  $\sigma_r = \sigma_{max} - \sigma_{min}$ ,  $\sigma_e$  is the stress range after mean stress correction,  $\sigma_u$  is the ultimate strength. The Gerber method treats positive and negative mean stress correction in the same way that mean stress always accelerates fatigue failure.

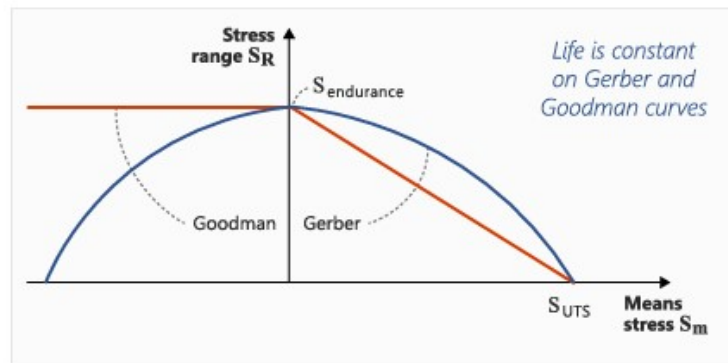


**Figure 5.10:** Haigh Diagram and Mean Stress Correction Methods

The load cycle history often does not follow a clear sinusoidal trend; thus, it's important to have a solid algorithm that can count the cycles to assess which are the amplitudes and the mean or pick stresses. The most widespread counting method is the Rainflow. It requires that the stress time history be rearranged so that it contains only the peaks and valleys, and it starts either with the highest

peak or the lowest valley (whichever is greater in absolute magnitude). Then, three consecutive stress points (1, 2, and 3) will define two consecutive ranges as  $\Delta\sigma_{12} = |\sigma_1 - \sigma_2|$  and  $\Delta\sigma_{23} = |\sigma_2 - \sigma_3|$ . A cycle from 1 to 2 is only extracted if  $\Delta\sigma_{12} \leq \Delta\sigma_{23}$ . Once a cycle is extracted, the two points forming the cycle are discarded, and the remaining points are connected. This procedure is repeated until the remaining data points are exhausted.

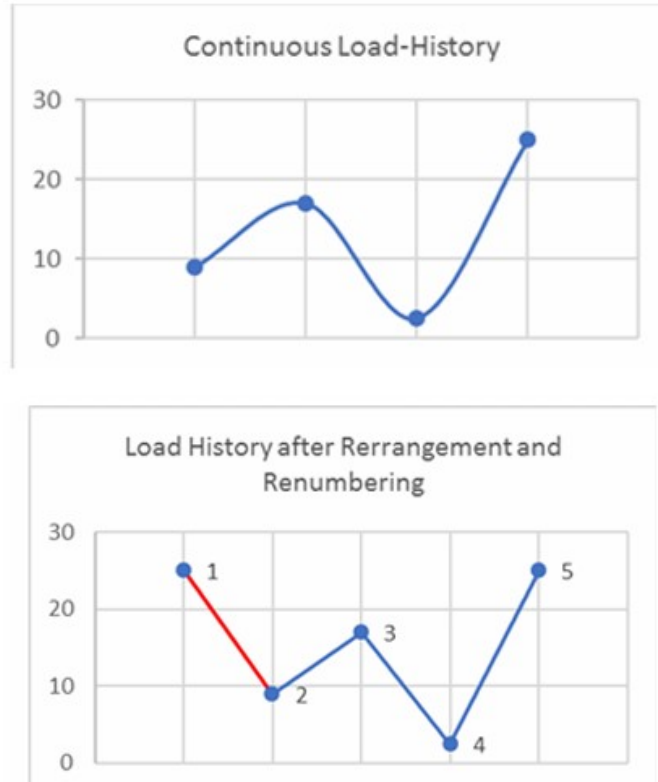


**Figure 5.11:** Load cycle before and after Rainflow arrangement

Since the S-N theory deals with uniaxial stress, the stress components need to be resolved into one combined value for each calculation point at each time step and then used as equivalent nominal stress applied on the S-N curve. Various stress combination types are available, with the default being "Absolute maximum principles stress.". "Absolute maximum principle stress" is recommended for brittle materials, while "Signed von Mises stress" is recommended for ductile material. The sign on the signed parameters is taken from the sign of the maximum absolute principal value.

Concerning the output of the model, we have two different types of results. The safety factor and the damage. The damage is used to predict when a certain

component will fail or how impactful a load cycle history is on the component. There are different calculation methods, but the easiest and most used is the Palmgren-Miner method. Palmgren-Miner's linear damage summation rule is used. Failure is predicted when:

$$\Sigma D_i = \Sigma \frac{n_i}{N_{if}} \geq 1.0 \quad (5.4)$$

Where  $N_{if}$  is the material fatigue life (number of cycles to failure) from its S-N curve at a combination of stress amplitude and means stress level  $i$   $n_i$  is the number of stress cycles at load level  $i$ .  $D_i$  is the cumulative damage under  $n_i$  load cycle. The linear damage summation rule does not take into account the effect of the load sequence on the accumulated damage due to cyclic fatigue loading. However, it has been proven to work well for many applications.

The Safety Factor is used to predict if a certain component will fail at a specific number of cycles; in fact, it's calculated based on the endurance limit or target stress (at target life) against the stress amplitude from the working stress history. If the mean stress is constant, the Gerber model gives us:

$$SF = \frac{\sigma_e}{\sigma_{a0}} \quad (5.5)$$

where  $\sigma_{a0}$  is the stress amplitude after mean stress correction.

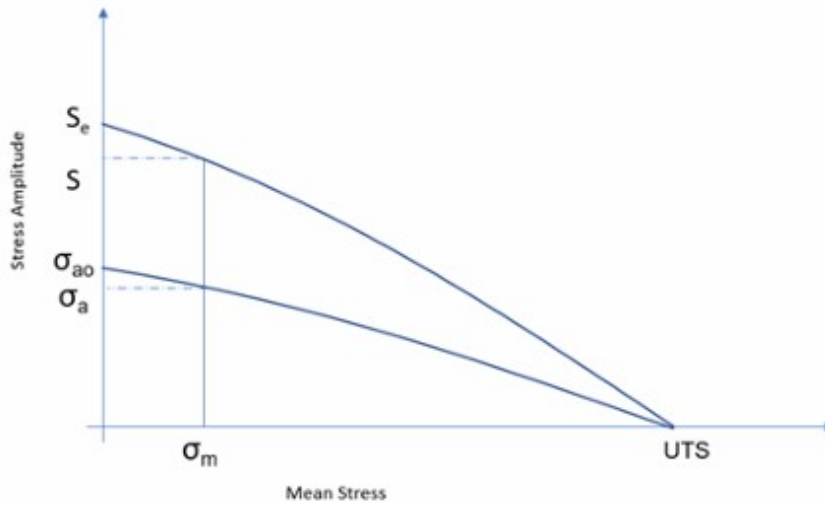


Figure 5.12: Gerber Safety Factor

## Chapter 6

# Design for Additive Manufacturing

In the 2.3 section, we discussed why the design process must be carried out using additive manufacturing. Now, it is time to give a little more specifics about additive manufacturing. As for the other topics, the goal of this work is not to report all the state-of-the-art of this technology. The aim is to identify the most important characteristics needed to fabricate a component using additive manufacturing.

The chapter's name is designed for additive manufacturing, which includes all good practices for fully exploiting AM's characteristics. Design for additive manufacturing has been developed to guide designers in the feasibility of their designs, introducing constraints during the design stage. An integrated approach between design and manufacture involves first considering the optimal design and then applying the geometric simplifications needed to make manufacturing feasible. The principles of DfAM can be summarized as follows:

- ///* Do not consider the conventional design approach
- ///* Capitalize the capabilities of AM technologies
- ///* Rethink the whole assembly towards integrated freeform design
- ///* Use as little raw material as possible to optimize the design towards the highest strength and lowest weight
- ///* Feel free to use freeform designs; use undercuts and hollow structures if they are useful
- ///* Design the optimal shape of the part according to functionality

For the reasons explained, topology optimization is particularly suitable for AM applications. However, design is always the result of a trade-off between functional requirements and manufacturing requirements. It is fundamental to have a good knowledge of the process that will be used to produce the products to design the part at the best.

## **6.1 Processes and Materials for Additive Manufacturing**

Additive manufacturing is a process by which 3D CAD data is used to manufacture components layer-wise by depositing materials, which can be metals, plastics, composite materials, etc. '3D printing' is used as a synonym for Additive Manufacturing. AM usually starts with the application of a thin layer of material (for example, powdered metal), which can be as thin as 100 microns, onto a building platform. A robust ray (a laser or electron beam) then fuses the powder at precisely the points and paths defined by the CAD data. Then, the platform is lowered, another layer of powder is applied, and the whole process is repeated until the component is fully formed.

In this work, we focus on the processes called powder bed fusion (PBF).

Laser Powder Bed Fusion (L-PBF) is an advanced additive manufacturing (AM) technique that selectively melts fine metal powders using a laser, building fully dense parts layer by layer.

The process begins with a thin layer of metal powder deposited on a building platform using a recoater blade, typically made of ceramic or metallic materials. The excess powder is collected by a dedicated collector. A high-power laser, often a fiber laser with a 400 W output (ranging from 100 W for small systems to 1000 W for high-productivity machines), selectively melts the powder based on the cross-sectional geometry of the part. The platform is lowered after each layer by a distance equal to the thickness of the layer, and the sequence repeats until the entire part is formed. Laser focusing is achieved using an F- $\theta$  lens with a typical spot size of 0.1 mm, though some machines allow dynamic adjustment of spot size to optimize detail and productivity.

The process operates in a controlled inert atmosphere, typically using nitrogen or argon, to prevent oxidation of powder. A continuous gas flow removes smoke and fine particles generated during melting, ensuring optimal laser performance and preventing chamber contamination.

The temperature of the building platform is maintained between 40 ° C and 250 ° C well below the melting point of the material, resulting in significant thermal gradients. These gradients lead to high residual stresses in the parts, making them susceptible to warping or curling. To mitigate these effects, parts are anchored to

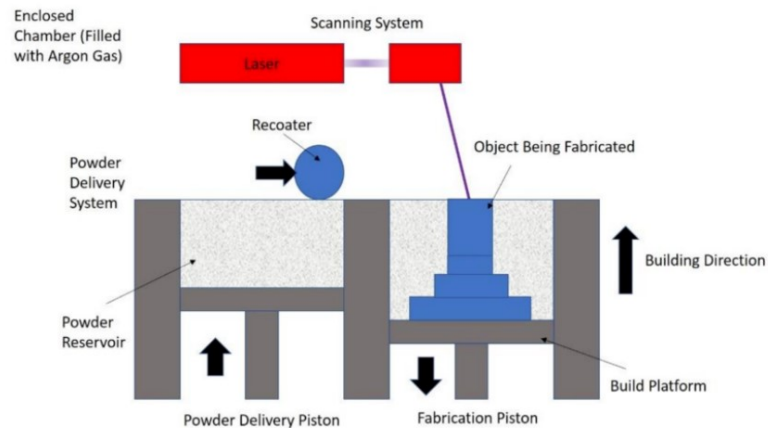


**Figure 6.1:** Schematization of a Laser Powder Bed Fusion process

the platform and supports are added to enhance heat transfer and prevent local overheating, especially in overhanging regions. Post-processing, such as thermal stress relief treatments, is required to stabilize the parts before removal from the platform [9].

### 6.1.1 Best practice for Additive Manufacturing

As said above, this work aims to describe the design process of a component using additive manufacturing. Thus, we will not go further in detail concerning the technology, knowing that the concepts discussed are not enough to have a full theoretical basis on the subject. Nevertheless, it's more interesting to focus the attention on tips and good practices that must be followed when we are designing something using additive manufacturing, especially metals through LPBF.

In the LPBF process, the simplest geometry to fabricate is a vertically extruded shape from the build platform, where each layer is deposited directly above the previous one. This approach minimizes the likelihood of issues occurring during the build process. However, as the geometry becomes more complex, such as in the case of inclined surfaces or more intricate shapes, additional design considerations must be taken into account. One of the primary challenges in design is dealing with inclined surfaces, as the powder in the build chamber does not provide any support during the material fusion. Therefore, inclined surfaces should ideally be designed to be self-supporting, meaning they must have a minimum angle concerning the horizontal plane to avoid requiring additional support structures.

The minimum angles required to ensure surface stability and thus avoid the need for supports vary depending on the material. Typical values are as follows:

/// Stainless steel: 30°

/// Inconel: 45°

/// Titanium: 20–30°

/// Cobalt-chrome: 30°

Thus, titanium is the least critical material for creating self-supporting surfaces, while Inconel and aluminum are the most critical, as they require higher angles to ensure stability. If the angle is too steep, it will necessitate the inclusion of support structures within the model, which will then need to be removed via machining or wire cutting, increasing both energy consumption and material use. Furthermore, if the angle is near the threshold for self-supporting, the downward-facing surface may exhibit roughness (commonly called the stepped appearance), which requires additional post-processing. In addition to supporting non-self-supporting surfaces, supports are crucial for anchoring the part to the build platform and minimizing distortions during the build process.

Another important aspect is the design of horizontal holes in the part. Small holes, typically less than 6 mm in diameter, can be accommodated without requiring support structures, regardless of the material used. However, larger holes will require support structures to prevent the part from collapsing or becoming distorted during the build. These supports, as with inclined surfaces, must be removed post-build via wire cutting or machining. If the hole has an angled or arched upper section, it may not require support. However, this solution could lead to stress concentrations at the tip of the arch, potentially reducing the part's fatigue resistance.

The interaction between the recoater blade and the part is another critical factor in the LPBF process. If the blade does not move over the part progressively and smoothly, it may lead to problems. This is particularly important if the recoater blade is made of metal or ceramic, as these materials have higher rigidity. When the recoater blade passes over the part, depositing a new layer of powder, it can apply force to the previous layer. Therefore, part orientation plays a significant role in minimizing such issues. The ideal geometry is a circular profile, which provides a smooth lead-in for the recoater blade and a stable cross-section as the part builds. An open U-shape is also ideal, provided the recoater operates in only one direction, as the lead-in for the blade will again be rounded and the basic profile will be strong enough to resist the force of the recoater.

Thin sections parallel to the recoater blade's direction are problematic because the blade will tend to bounce off the parallel walls, and the thin section itself will not be able to resist the force of the blade as it builds. Any flat surfaces should be angled at least 5° from being parallel to the recoater blade to ensure that the blade contacts the part at a point rather than a flat face. Additionally, inherently stiff geometries are better suited for LPBF, as they can resist bending forces during

recoating. For this reason, orienting the part to minimize the contact area between the part and the recoater blade is beneficial, as it maximizes the bending stiffness of the part about the blade's action.

The bending moment applied to the part increases as it gets taller. As a general guideline, the ratio between the section and height should not exceed 8:1. The exact proportions depend on the specific geometry, but if the section becomes too high, there is a risk that the recoater blade will cause the part to bend, possibly damaging the part or the blade itself and terminating the build. To prevent these issues, slender geometries must be bridged at certain points with supports to increase the part's stiffness during fabrication. Arches are the best way to achieve this without creating downward-facing flat surfaces.

Even geometries that will be structurally sound when completed may need temporary support during the build process. For instance, triangular sections that are weak near the apex might require support structures in the middle to provide stability before the part is completed. If the open structure is intended for weight reduction, perforating it with small holes (preferably under 6 mm in diameter) may help reduce weight without requiring additional support.

Other key considerations involve avoiding sharp edges, thick sections, and angles that face the recoater blade. Sharp edges cannot be built in LPBF, and parts should be designed with minimum radii of around 0.5 mm to avoid stress concentrations, which can lead to part failure. Similarly, thick sections in the horizontal plane can cause issues related to heat buildup, particularly with materials like titanium. The best approach is to angle the part to minimize horizontal sections at any time, reducing residual stresses and improving the building geometry.

Angles facing into the recoater blade's path should be avoided, as this can cause the blade to collide with the part, potentially terminating the build. The ideal orientation allows for an angled contact between the blade and the part, which minimizes the risk of collision and maximizes the stability of the geometry.

Supports are an unavoidable aspect of the LPBF process but should be minimized wherever possible, as they consume significant energy during both construction and removal. Supports serve several vital functions, such as:

-  Supporting newly melted surfaces, particularly on downward-facing and shallow-angled surfaces
-  Preventing deformation of the new geometry
-  Dissipating heat away from the freshly formed part
-  Providing temporary support for geometries that are weak during the build but strong once completed

The ideal design requires no support at all. In reality, however, it is rare to achieve this, so the challenge lies in minimizing the need for support to save time,

energy, and cost. Reducing support structures not only saves time during the build but also post-processing. While support structures can be automatically added to the CAD model by specific software tools, manual adjustments are often necessary to optimize their shape and position. Minimizing the number of supports also reduces the time spent on these adjustments and ensures that less post-processing time is required.

The most common types of support include:

- ✍ **Simple fill-in supports:** These are the simplest forms of support, filling in the necessary areas and then being removed by wire cutting or machining when the build is complete
  
- ✍ **Offset supports:** These structures rise vertically and then angle in to support specific surfaces. They require less machining and are usually removed by wire-cutting the base of the part
  
- ✍ **Supports for overhanging surfaces:** For non-self-supporting surfaces, the simplest solution is to support them from the base. However, this approach consumes more material and energy

A better solution is to use buttress supports, which connect the overhanging surface to the main geometry at an angle, thus reducing material use. Strong support structures help minimize the buildup of stresses within the part, which is particularly important in LPBF, as the high temperatures involved in the process can lead to significant internal stresses. These stresses can result in delamination, cracks, distortion, and warpage during post-processing. These issues can be mitigated by heat treating or shot-peening the part before removing it from the build platform.

Incorrect design of the part or support structures can also lead to stress buildup, which can cause detachment of the supports from the platform and of the part from the supports. This misalignment can lead to distortion, changing the part's orientation and geometry, and possibly causing collisions with the recoater blade.

Minimum wall thicknesses vary depending on the material but generally should not be below 1 mm. In the case of LPBF, this also depends on the minimum laser spot diameter. Thin wall sections or placing thin sections adjacent to thick sections can result in significant distortion due to the high temperatures involved in the process.

While fine details like small holes are achievable, especially in the vertical plane, threads are generally produced during post-processing rather than directly in the build process. Threads should be designed vertically with adequate clearance around the thread to allow post-processing (e.g., tapping or thread milling).

### 6.1.2 Metallic materials for Additive Manufacturing

One of the most important aspects of mechanical design is the choice of material. This choice is subordinated to the chosen production process; additive manufacturing and traditional processes exploit different materials. In the 2.2 we gave already some hints about generic material properties, but in this section, we can formalize the material choice.

Aluminum alloys are the best choice for this application; they guarantee the best trade-off between lightweight, stiffness, and cost. The main drawback is the strength of the aluminum alloy used in the SC21 and, in general, used in AM.

The main issue with aluminum alloy strength produced with PBF is stress-relieving; in industrial applications, it's quite common to perform stress-relieving after the printing because the AM process tends to leave a high amount of residual stress in the component. The stress-relieving increases the grain size of the material and improves the elongation at fracture but worsens the strength.

In addition, most of the high-strength aluminum alloys are not processable by AM processes because they are highly crack-sensitive. The content of alloying elements like silica and magnesium is generally somewhere close to the values that correspond to peak crack sensitivity.

A high-strength material used in industries is scalmalloy, which has high specific strength and stiffness. It is a hypereutectically scandium (Sc) alloyed AlMgMn. The principle on which this material relies is the supersaturation of the AlMg matrix with Sc and Zr; thus, fast cooling procedures during solidification are fundamental to freezing the supersaturated state to room temperature. Overall, Scalmalloy has:

- ✄ High tensile properties. High fatigue properties.
- ✄ Exceptional high corrosion resistance.
- ✄ Robust manufacturing chains.
- ✄ High toughness.

The only issue related to the use of this alloy is its quite high cost, which is due to the presence of Sc and Zr [9].

The alternative for this application to aluminum alloys is Ti64. Titanium Ti64 is a Ti6Al4V alloy known for its low density, high strength, and excellent corrosion resistance. It offers higher fatigue resistance than other lightweight alloys and is lighter than superalloys and steels. Parts made from Ti64 can be machined and polished in both as-manufactured and heat-treater states. Due to the layerwise building method, parts may exhibit anisotropy; heat treatment is recommended to reduce internal stresses and enhance ductility.

Taking into consideration also the AlSi10Mg with its characteristics, reported in 2.4 and in 2.2, we decided to use this aluminum alloy for its availability on

Properties	Values
Tensile strength	470 [MPa]
Yield strength	500 [MPa]
Young modulus	69 [GPa]
Elongation at break	8 [%]
Density	4.4 [ $g/cm^3$ ]
Hardness	74 [HRB]
Fatigue strength	180 [MPa]

**Table 6.1:** Scalmalloy mechanical characteristics.

Properties	Values
Tensile strength	970 (XY) / 1010 (Z) [MPa]
Yield strength	1080 (XY) / 1080 (Z) [MPa]
Young modulus	114 (XY)/ 114 (Z) [GPa]
Elongation at break	14 (XY)/ 15 (Z) [%]
Density	4.4 [ $g/cm^3$ ]
Hardness	30-35 [HRC]
Fatigue strength	595 [MPa]

**Table 6.2:** Ti64 Grade 5 mechanical characteristics.

the market and lower costs. In addition, a lot of tests and data are available for this material that help during the design phase. The limit fatigue life for a material is very difficult to assess because many experimental tests are needed. In the previous chapter, we saw that the S-N diagram is mandatory for a fatigue analysis. The information about the maximum number of cycles before failure and the corresponding stress is very difficult to find. In our case, the S-N curve was built starting from the value found in [10].

For these reasons, AlSi10Mg is the most suitable material for a complete design phase.

### 6.1.3 Post processing of an Additive Manufacturing component

Despite these advantages, the surface quality and tolerances achieved with AM technologies remain relatively low. Consequently, an as-built AM part is rarely considered “finished” once the build process is complete. Tolerances are comparable to those achieved through casting (approximately 1 mm), and surface roughness tends to be significant. Therefore, finishing treatments are essential to refine the part’s geometry and improve fatigue performance, which is adversely impacted by the inherent surface characteristics of metal AM parts.

The typical post-build workflow includes heat treatment (to relieve residual stresses), separating the part from the build platform, transferring the part to a CNC machine, and performing the machining process. It is crucial to relieve residual stresses before machining; otherwise, stress release during machining can distort the part. Each component is machined individually, even when multiple parts are produced on the same platform.

The goals of finishing processes include enhancing aesthetics, achieving dimensional accuracy, reducing surface roughness, improving mating surfaces and features, enhancing part functionality, optimizing tribological properties, and extending fatigue life. If the objective is to reduce roughness while tolerances are less critical, abrasive finishing processes can be employed.

However, when tight tolerances are mandatory, machining with CNC machines becomes the only viable option. The combination of additive and subtractive manufacturing techniques is known as hybrid manufacturing (HM).

Implementing HM is complex due to the inherent differences between additive and subtractive processes:

**⚡ Holding and fixing challenges:** The complexity and roughness of AM surfaces make it difficult to secure parts in the machine. Establishing datums and reference points for orienting and locating the part, as well as defining tool paths for the CNC machine, becomes particularly challenging after the part is separated from the build plate.

**⚡ Vibration issues:** The low stiffness of AM parts can lead to vibrations during machining, reducing accuracy. While this may seem counterintuitive, it arises from the fact that AM parts are optimized for specific functional loads, resulting in low stiffness for other types of loads. To address this, additional features can be incorporated into the design to enhance stiffness during machining, or machining loads must be considered during the design’s optimization phase.

**⚡ Access limitations:** Intricate geometries may restrict access to certain areas with cutting tools.

To summarize, AM parts often require post-processing due to their low surface quality and tolerances, which are comparable to casting (about 1 mm). Finishing treatments like heat treatment, CNC machining, or abrasive processes are necessary to refine geometry, reduce surface roughness, and improve performance. HM, combining additive and subtractive techniques, is a potential solution but poses challenges such as fixing and holding complex parts, managing low stiffness (which causes vibrations), and accessing intricate geometries. Proper design considerations can mitigate these issues, ensuring better machining outcomes.

Thus, it's important to adjust the shape of the component in a way that a traditional CNC machine can operate easily. Unfortunately, it's not an easy task because there's the risk of not fully exploiting the AM possibility. On the other hand, it can happen to increase too much the costs or the complexity of the CNC process. It's possible, for example, to introduce some sacrificial supports. These structures aim to secure the component in the CNC machine, providing support to be cut away at the end. It is very difficult to take into account these problems during the design phase because the production of support is usually automated by the software, and it is challenging to modify the shape as you want.

It is clear that it is important to speak with professionals in the sector who can give you advice, especially on how to block the component in the CNC machine and which surface should be used as a reference.

# Chapter 7

## Results

### 7.1 Topology optimization results



**Figure 7.1:** Final upright model

The final model of the upright is shown in 7.1. We can see how the material is concentrated in the lower part, whereas the upper part is more hollow and thinner. It is important to note that the optimization process often requires more than one run of the software. Trial and error are the only way to properly tune the different parameters, such as stress constraint, element size, minimum element thickness, and % of volume. In addition, it is good practice to start with a bigger design space and a % of remaining volume around 50 %. In this way, the constraint is not too

stringent, and the analysis turns out to be more precise and less prone to error. It is preferable to run more iterations starting from the output volume of a precedent analysis so that it is easier to get a coherent volume without disconnected parts.

Two main problems arise during the topology optimization. The first is the possibility of getting a noncoherent volume; in other words, parts of the material are not directly connected. This is clearly a result of the mathematical part of the solver that tries to optimize without a real consciousness of the components' physical behavior. As said, to avoid this problem repeating different times, the optimization with a larger remaining volume is advisable. In addition, trying to increase the design space can be a solution, but it's not always a complete answer because increasing the starting volume too much can make it more difficult to get the desired weight. Moreover, it's important to avoid perpendicular ribs concerning the direction of printing, not only because of the overhang but also because they are more prone to being disconnected by the software, especially in zones where they do not increase stiffness.

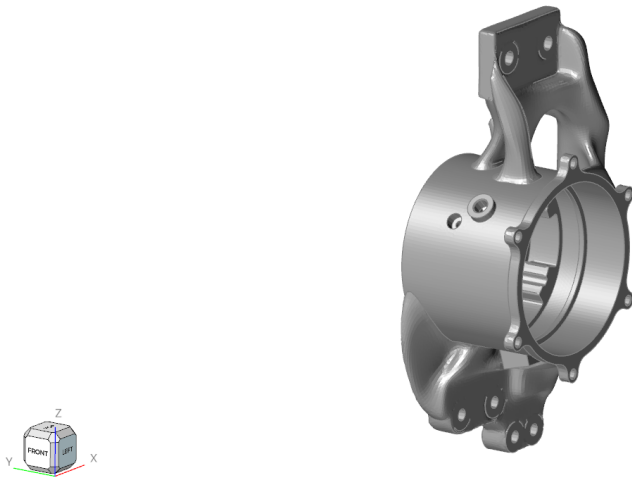


**Figure 7.2:** Final upright model lateral view

The second problem is to deal with the reconstruction of the optimized part. Inspire offers the polynurbs tool that can create a 3D part from the results, thanks to a mesh that shapes the component. This is always a critical step because it's often necessary to increase the number of elements, resulting in a very computationally heavy model. Unfortunately, this is the only available tool; thus, a trial-and-error phase is mandatory. Ultimately, exporting the model in CAD software and creating a step file can be an alternative, but it's not always possible.

The results show that the weight target is not satisfied. This can be explained

Final upright weight [g]	SC24 upright weight [g]
1244	895

**Table 7.1:** Comparison between the optimized upright weight concerning the SC 24 one

better in the next chapter, where we will see the results of the safety factors. The structural integrity and reliability, as said before, are the main outputs of a mechanical component. In this case, the trade-off is found in increasing the weight but respecting the structural and stiffness targets set.

Moreover, the results are directly linked to the strength of the material that is lower than the ones of the other aluminum alloys reported in chapter 6. In this case, the aspect that should be taken into consideration is the cost and availability, which are strong points of the AlSi10 compared to the other alloys.

Ultimately, a further optimization could have been carried out, but not without reducing the structural targets already set.

## 7.2 Reliability model results

The reliability model's main output is the Von Mises stress. The formulation of the Von Mises stress is the following:

$$\sigma_{VM} = \frac{1}{\sqrt{2}} \sqrt{(\sigma_1 - \sigma_2)^2 + (\sigma_2 - \sigma_3)^2 + (\sigma_3 - \sigma_1)^2} \quad (7.1)$$

The previous equation is used with the principal stress; thus, the condition where the shear stresses are null. The peak Von Mises stress is then compared with the yield strength of the material 2.2 to obtain the safety factor. This operation is then repeated for each load case.

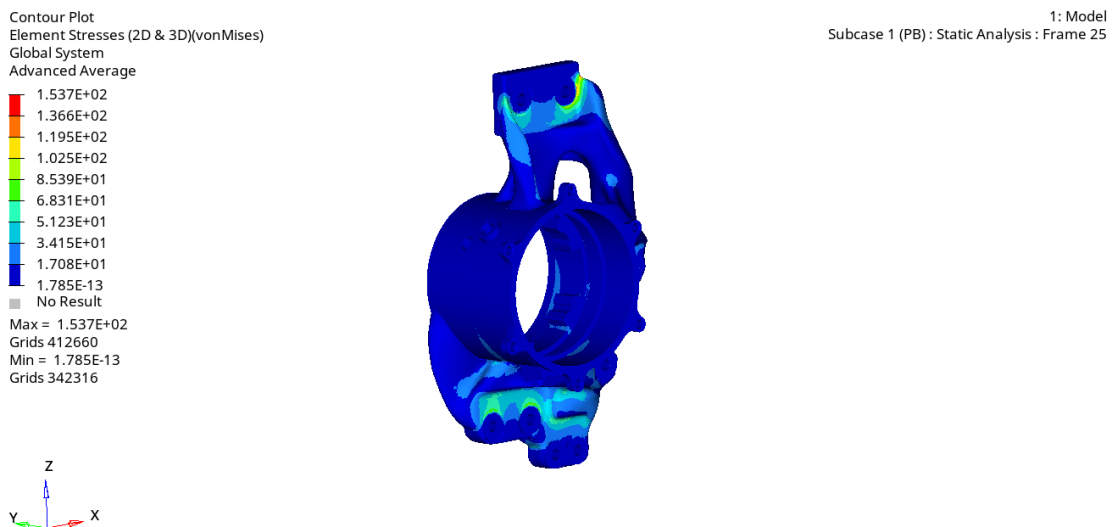


**Figure 7.3:** Von Mises stress [MPa] for the pure braking load case

The worst part is in the top right corner, where a stress concentration is present. It's probably a local concentration due to the presence of the RBE2 with the constraint. The RBE2 rigidly connects the elements to the single-point constraint, adding unwanted stiffness to the model.

This can only partially explain the problem; a relevant contribution to the concentration of stress is due to the sharp geometry change. It's very likely that adding a fillet or reducing the curvature at that point can be beneficial in terms of peak stress.

The previous figure 7.4 displays the signed Von Mises stress, which represents the Von Mises stress with the sign of the maximum principal stress of the element. The figure tells us which elements are in tension and which are in compression. We can see that the corner is in tension that spreads to the lower part of the hole,

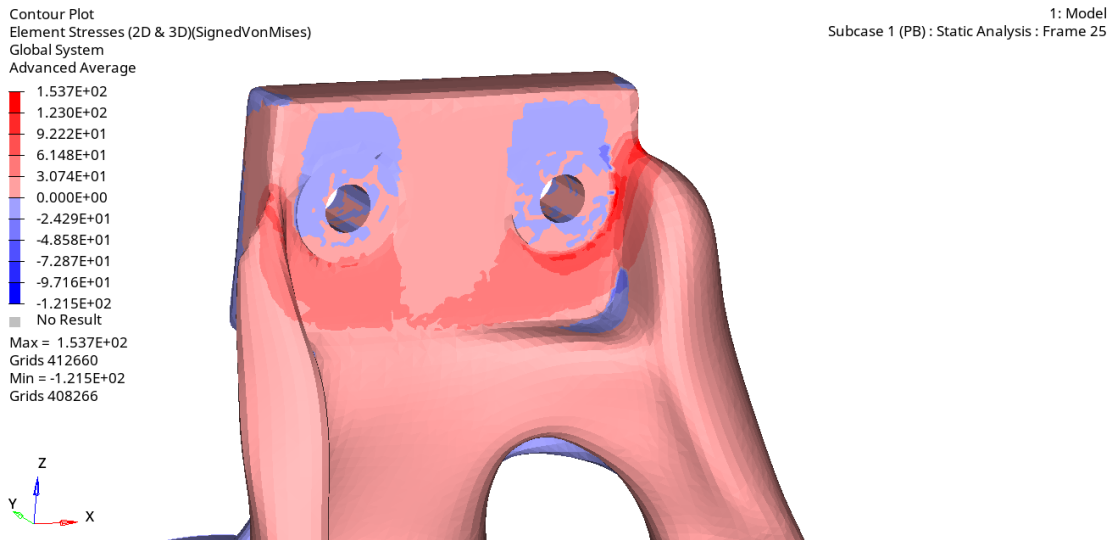


**Figure 7.4:** Signed Von Mises stress [MPa] pure braking load case

whereas the upper part is in compression. The RBE2 application partially worsens this behavior, but the next figure can give us more details.

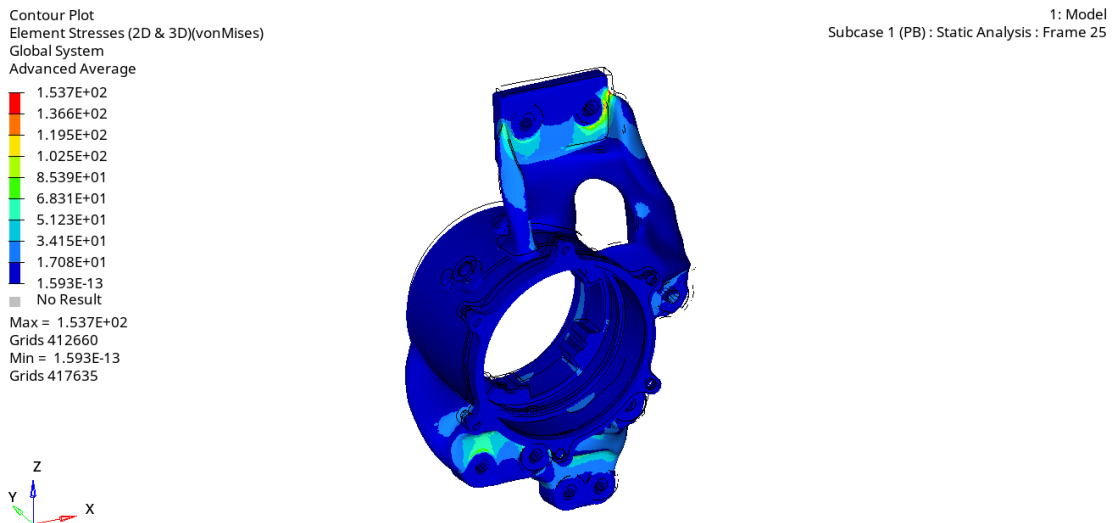


**Figure 7.5:** Deformation results pure braking load case

The 7.5 shows us the deformation of the component concerning the unloaded condition. The stretching of the elements present in the top right corner is due to a certain torsion explained by the presence of the braking caliper forces. After this analysis, we can conclude that a different application of the RBE2 could help, but

a fillet or a variation in the component's geometry could be an option.

In the following figures 7.6,7.7 we can see the results for the other load cases.

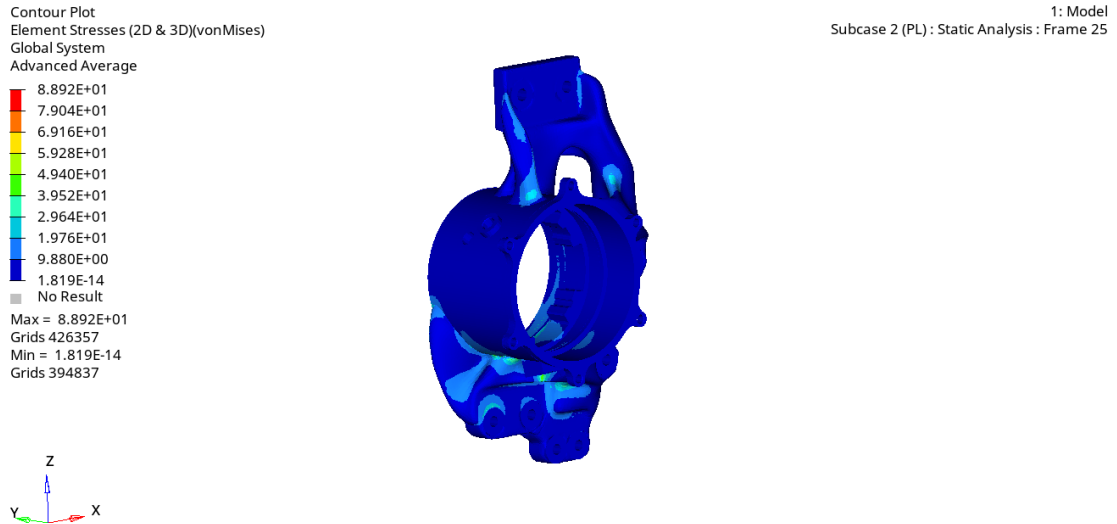


**Figure 7.6:** Von Mises stress [MPa] for the pure lateral load case

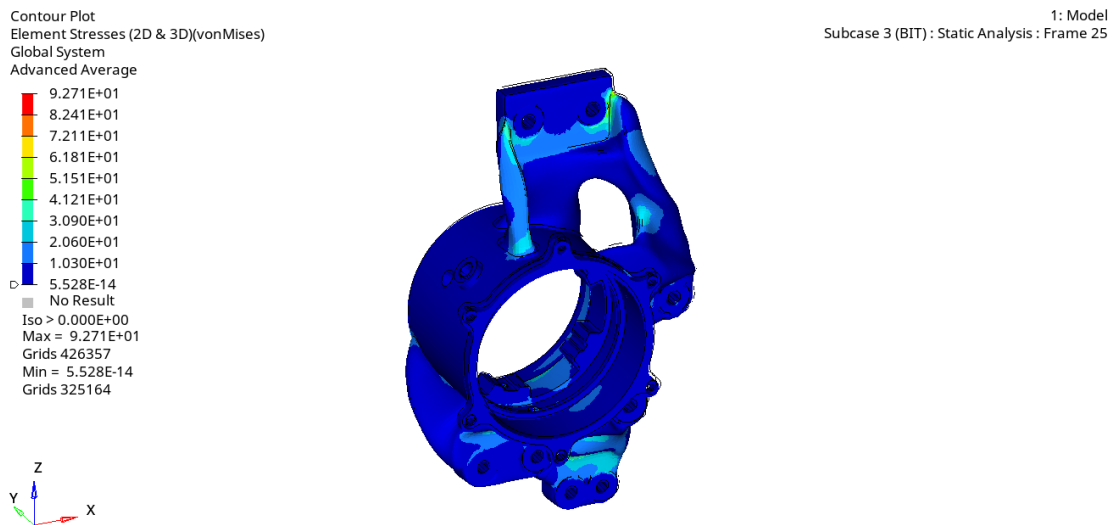


**Figure 7.7:** Von Mises stress [MPa] for the braking in turn load case

Some further considerations can be done for the pure lateral load cases. We can see that the top corner is not particularly stressed; this is due to the different deformation of the component provoked by the absence of the caliper forces. As we can see in the following 7.8

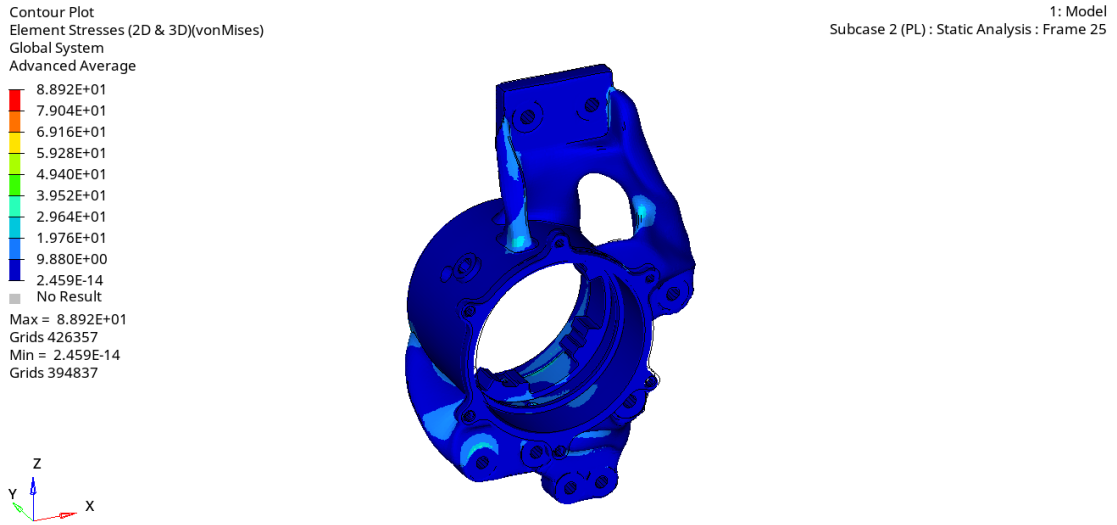


**Figure 7.8:** Deformation results pure lateral load case

Peak PB stress [MPa]	Peak PL stress [MPa]	Peak BIT stress [MPa]
154	89	92

**Table 7.2:** Results sum up of the peak stresses for the three different load case

Target Safety factor	Safety factor PB	Safety factor PL	Safety factor BIT
2.5	1.75	3	3

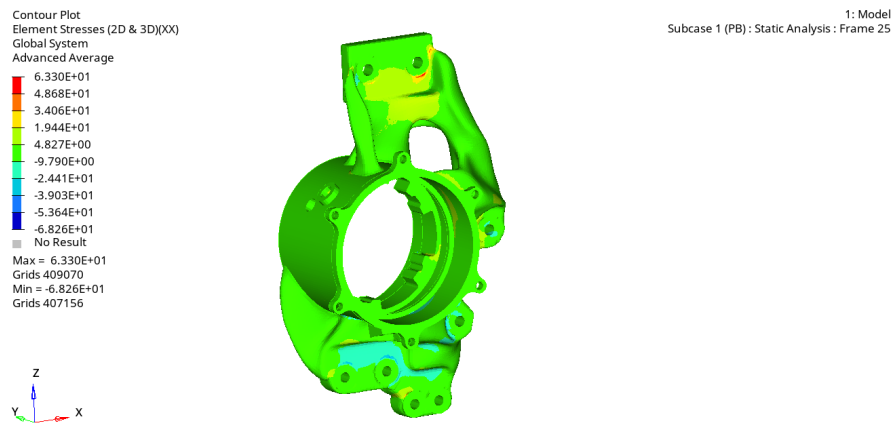
**Table 7.3:** Safety factor for the three load cases

As we can see, the safety factor is not satisfied for the pure braking load case. We already discussed the reasons why, and it's necessary to have a variation in the top corner of the component. To understand how efficiently to modify the structure of the component, it is important to know which stress component has the biggest impact.

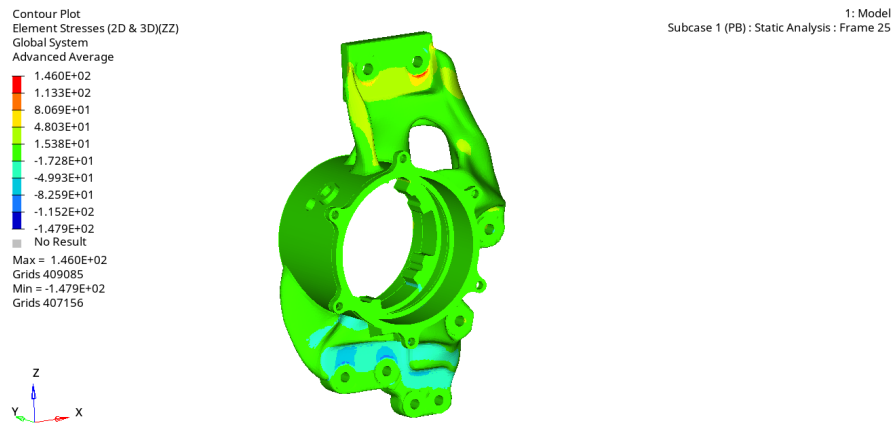
Referring to the type of deformation of the component, we expect that the main components are the X and Z directions. The deformation and, consequently, the stresses depend on the caliper's forces acting along these two directions.

The X component is significantly lower both for the magnitude of the force vector and for the small distance in the lateral direction between the force and the interested zone.

To reduce the impact of the Z component, a structural reinforcement in the



(a) X component of the stress in the pure braking load case



(b) Z component of the stress in the pure braking load case

**Figure 7.9:** Stress components in the pure braking load case

vertical direction is needed 7.10; otherwise, if the X component had been more significant, a reinforcement perpendicular to the zone would have been necessary.

Model Info: C:/Users/franc/Desktop/TESI/Lavoro/Analisi/Hypermesh/PB\_modifica.hm\*

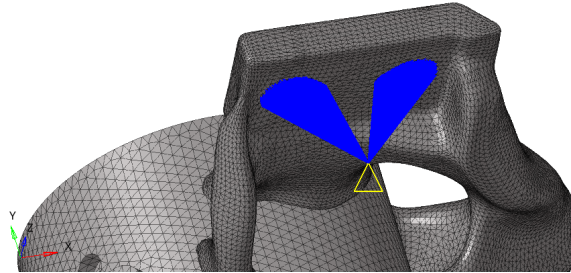


**Figure 7.10:** Geometry variation to reduce the stresses in the pure braking load case

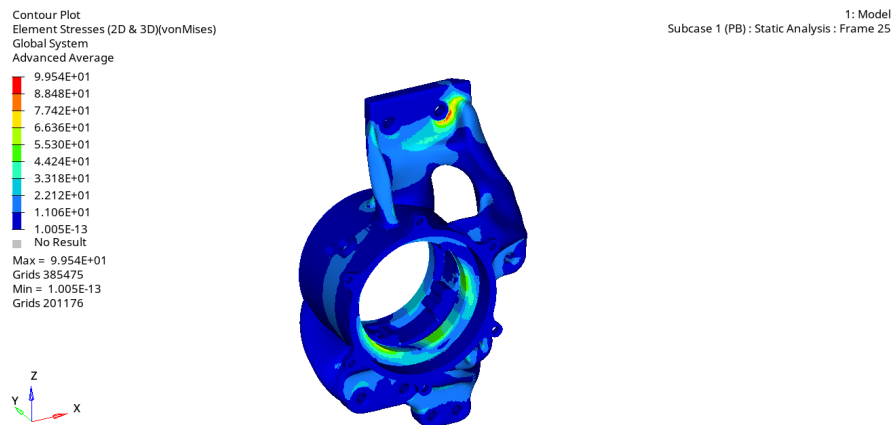


**Figure 7.11:** Von Mises stresses in the pure braking load case after the variation

Another analysis was performed 7.11, and the results show a significant stress reduction following the safety factor target 7.4.

Peak PB stress	Safety factor target	Safety factor PB
103	2.5	2.6

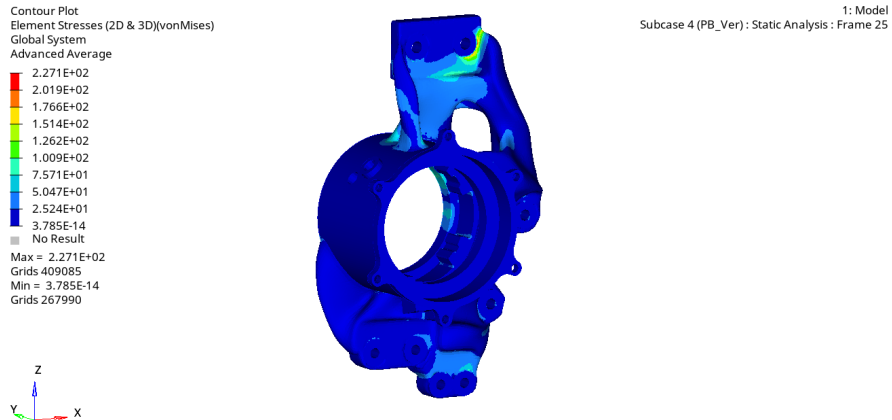
**Table 7.4:** Safety factor for the pure braking load case after the variation

### 7.2.1 Verification analysis results

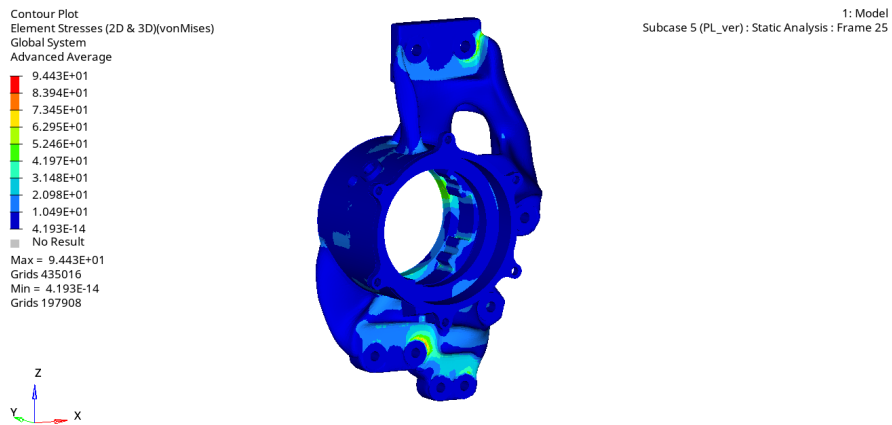
The same procedure has been carried out with verification load cases.

Target SF	SF PB	SF PL	SF BIT
1	1.2	2.8	3.3

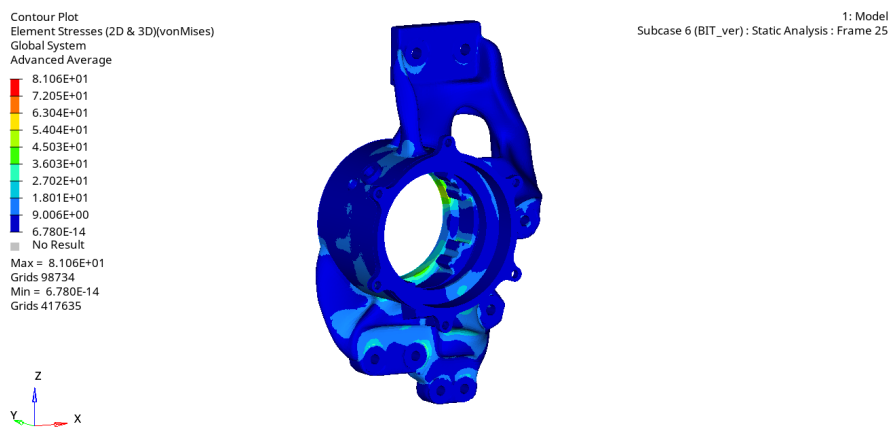
**Table 7.5:** Safety factor for the three load cases verification model



(a) Von Mises stresses pure braking verification case



(b) Von Mises stresses pure lateral verification case



(c) Von Mises stresses braking in turn verification case

**Figure 7.12:** Von Mises stress in the verification load case

### 7.3 Stiffness model results

The main output of the stiffness model is the coordinate variation of the three points used to compute the characteristic wheel angles. The three points are not a part of the component; thus, the displacements displayed in figures 7.13 are not directly indicating the coordinate variation.

A tool can identify the coordinates of a node tracked by its ID number.

We can now show the variation of coordinates in the different cases, referring to 5.1

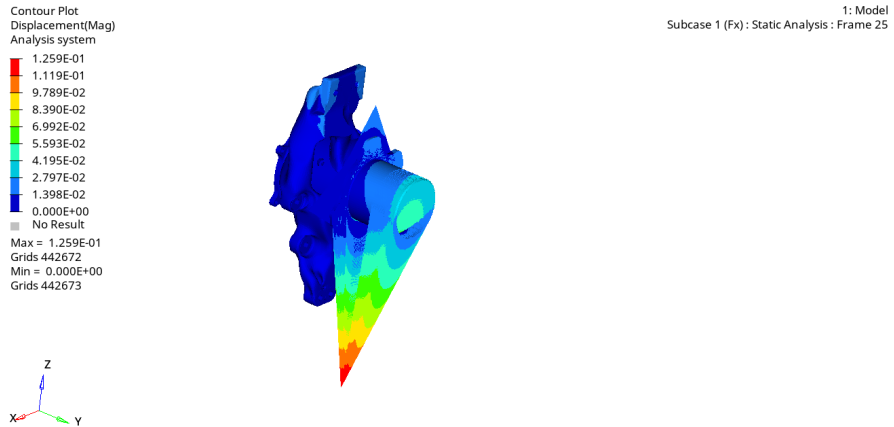
Points	X [mm]	Y [mm]	Z [mm]
Wheel center	-0.006	600.999	-0.001
Wheel system X	99.994	601.005	0.010
Wheel system Z	-0.017	600.999	99.999

**Table 7.6:** Coordinates of the three points after the deformation Fx load case

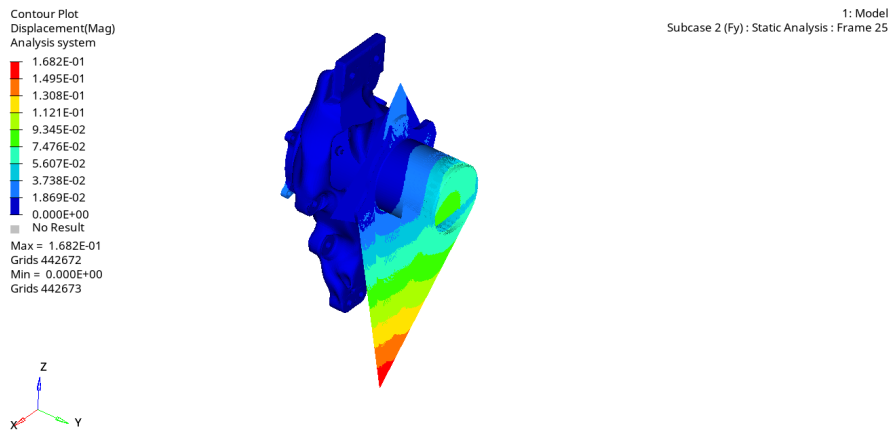
Points	X [mm]	Y [mm]	Z [mm]
Wheel center	-0.006	601.003	-0.005
Wheel system X	99.994	601.009	-0.003
Wheel system Z	-0.008	600.98	99.995

**Table 7.7:** Coordinates of the three points after the deformation Fy load case

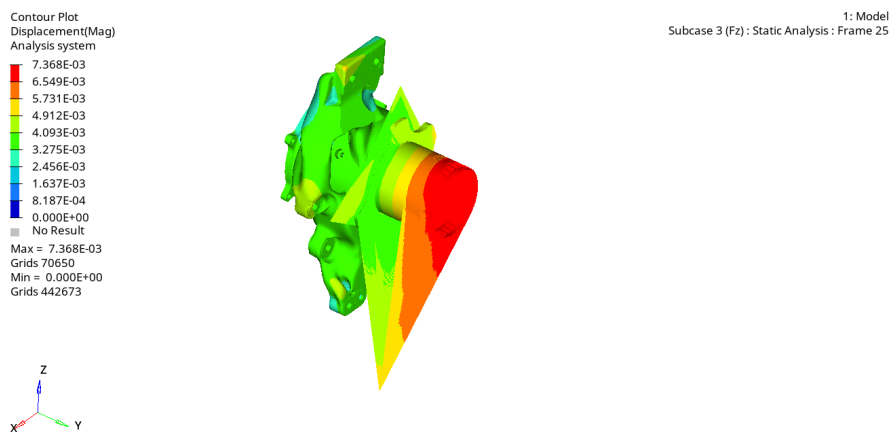
To compute the actual angle variation, we have different ways; the easiest is to put them in CAD software with the upright in the static position. After generating the geometry features needed, we can measure the distances and the angles to determine camber and toe variations. Alternatively, this computation can be done using a proper script in Matlab.



(a) Displacements results of the force in the longitudinal direction



(b) Displacements results of the force in the lateral direction



(c) Displacements results of the force in the vertical direction

**Figure 7.13:** Displacements results of the stiffness model

Points	X [mm]	Y [mm]	Z [mm]
Wheel center	0.002	600.999	0.003
Wheel system X	100.002	600.996	0.001
Wheel system Z	0.003	601	100.003

**Table 7.8:** Coordinates of the three points after the deformation Fz load case

Loads	$\Delta$ Camber target [deg/kN]	$\Delta$ Camber [deg/kN]
$F_x$	0.01	-0.002
$F_y$	0.01	0.0093
$F_z$	0.01	-0.0087

**Table 7.9:** Camber variation concerning the forces in the three directions x, y, and z respect to the targets

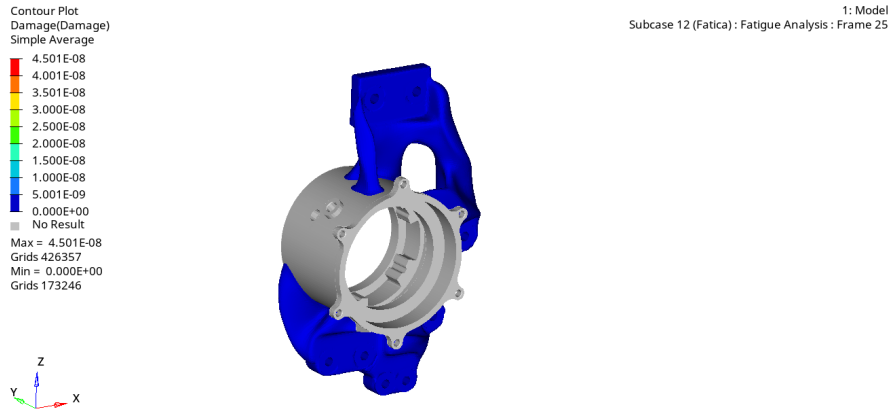
Loads	$\Delta$ Toe target [deg/kN]	$\Delta$ Toe [deg/kN]
$F_x$	0.01	-0.0063
$F_y$	0.01	-0.0084
$F_z$	0.01	-0.0034

**Table 7.10:** Toe variation concerning the forces in the three directions x, y, and z respect to the targets

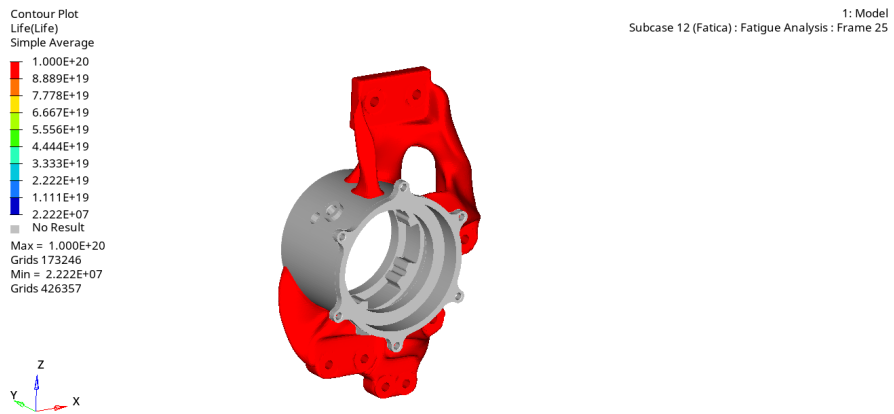
## 7.4 Fatigue analysis results

The output of the fatigue analysis deals with the amount of damage done by a simulation of an autocross lap made during track testing. A single lap is 500 meters long; thus, a relation between a distance and damage can be made.

As we can see, the damage is near 0; thus, we can conclude that the component is close to infinite life, especially considering that the input loads are the worst case possible in terms of performance.



(a) Damage result fatigue analysis results



(b) Safety factor fatigue analysis results

**Figure 7.14:** Fatigue analysis results

## Chapter 8

# Final considerations and future works

In light of the results and analyses presented in this thesis, we can now summarize the conclusions and identify potential improvements for future developments.

The objective of this thesis was to share the knowledge and skills acquired during the years spent in the racing team and apply them to a real case study—specifically, the upright manufactured using additive manufacturing.

This production method proved to be suitable for optimizing both the shape and material distribution to enhance the stiffness of the component. Moreover, the design freedom offered by additive manufacturing allowed the creation of geometries that would not have been possible with traditional manufacturing methods.

However, when analyzing the upright design for the SC24, a noticeable increase in mass was observed, negatively impacting performance. This increase is mainly due to two factors.

*✄* The first factor concerns the increase in structural targets, which resulted from the limited prior knowledge of the manufacturing method, leading to component failures in the past.

*✄* The second factor is related to the material used, which has lower structural performance compared to the material employed for the SC24 upright. This material was chosen because it is more readily available and less expensive than next-generation aluminum alloys specifically developed for additive manufacturing.

Regarding the structural targets, both in terms of reliability and stiffness, they were successfully achieved, mainly thanks to topology optimization. This technique, combined with the design freedom enabled by additive manufacturing, allowed for the attainment of the required stiffness and reliability.

In conclusion, the developed component has proven to be reliable and capable of ensuring sufficient stiffness at the cost of increased weight. Therefore, additive manufacturing does not appear to be the optimal choice for this particular component, mainly because a significant portion of it cannot be optimized due to the interface with the transmission. Furthermore, considering that the component would still require CNC machining for final modifications, the hybrid production approach appears to be inefficient.

This does not imply that additive manufacturing should be disregarded altogether. On the contrary, as this was an initial feasibility study, the results are encouraging, given that most targets have been met. With the support of industry professionals and experts in additive manufacturing, it would be possible to identify a more high-performance alloy, thereby reducing the gap with traditional manufacturing methods. Additionally, the knowledge gained on this production method could be beneficial in the future or for other components of the vehicle, where the design requirements might be different.

Finally, regarding future developments, the focus should be on developing testing methods for the component to validate FEM models. This practice is essential to ensure design reliability and could also help in reducing structural requirements, allowing for a greater focus on performance. In addition, enhancing the knowledge about additive manufacturing materials is key to unlocking the full potential of the production process.

# Bibliography

- [1] Giancarlo Genta and Lorenzo Morello. *The automotive chassis: volume 2: system design*. Springer Nature, 2019 (cit. on p. 7).
- [2] JR Davis. «Aluminum and aluminum alloys». In: *ASM international* (1993) (cit. on p. 13).
- [3] Matteis Paolo. «Course's note: material for lightweight design, Politecnico di Torino». academic year 2022/2023 (cit. on p. 14).
- [4] Alessandro Scattina. «Course's note: numerical model simulation part A, Politecnico di Torino». academic year 2021/2022 (cit. on p. 21).
- [5] Thomas Henry Gordon Megson. *Aircraft structures for engineering students*. Butterworth-Heinemann, 2016 (cit. on p. 22).
- [6] Derek Seward. *Race Car Design*. Bloomsbury Publishing, 2017 (cit. on pp. 22, 26, 29, 42).
- [7] Riccardo Pastorino. «Design of the Uprights Assembly of a Formula Student Prototype». PhD thesis. Politecnico di Torino, 2023 (cit. on p. 30).
- [8] Altair HyperMesh. «<https://2020.help.altair.com/2020/hwdesktop/hm/index.htm>» | Altair HyperWorks site help (cit. on p. 38).
- [9] Atzeni Eleonora. «Course's note: Additive and Design for Additive, Politecnico di Torino». academic year 2022/2023 (cit. on pp. 53, 57).
- [10] Vincenzo Paolo Leone. «Caratterizzazione meccanica avanzata di lega AlSi10Mg realizzata mediante additive manufacturing: studio del comportamento a trazione ea fatica= Advanced mechanical characterization of AlSi10Mg alloy made by additive manufacturing: study of tensile and fatigue behavior». PhD thesis. Politecnico di Torino, 2018 (cit. on p. 58).